High-Speed and High-Output InP–InGaAs Unitraveling-Carrier Photodiodes

Hiroshi Ito, *Senior Member, IEEE*, Satoshi Kodama, Yoshifumi Muramoto, Tomofumi Furuta, Tadao Nagatsuma, *Senior Member, IEEE*, and Tadao Ishibashi, *Senior Member, IEEE*

Invited Paper

***Abstract*—The unitraveling-carrier photodiode (UTC-PD) is a novel photodiode that utilizes only electrons as the active carriers. This unique feature is the key for its ability to achieve excellent high-speed and high-output characteristics simultaneously. To date, a record 3-dB bandwidth of 310 GHz and a millimeter-wave output power of over 20 mW at 100 GHz have been achieved. The superior capability of the UTC-PD for generating very large high-bit-rate electrical signals as well as a very high RF output power in millimeter/submillimeter ranges can lead to innovations in various systems, such as broadband optical communications systems, wireless communications systems, and high-frequency measurement systems. Accomplishments include photoreceivers of up to 160 Gb/s, error-free DEMUX operations using an integrated UTC-PD driven optical gate of up to 320 Gb/s, a 10-Gb/s millimeter-wave wireless link at 120 GHz, submillimeter-wave generation at frequencies of up to 1.5 THz, and photonic frequency conversion with an efficiency of −8 dB at 60 GHz. For the practical use, various types of modules, such as a 1-mm coaxial connector module, a rectangular-waveguide output module, and a quasi-optic module, have been developed. The superior reliability and stability are also confirmed demonstrating usefulness of the UTC-PD for the system applications.**

***Index Terms*—High-frequency measurements, high power, high speed, InP–InGaAs, millimeter wave, optical gate, photodiode, unitraveling-carrier photodiode (UTC-PD), wireless link.**

I. Introduction

PROGRESS in broadband and high-frequency photonic systems, such as high-bit-rate fiber-optic communications systems [1], fiber-radio wireless communications systems [2], and high-frequency measurement systems [3], demands innovative improvements in device performances. An optical-to-electrical (O/E) signal interface device is one of the key elements of these systems, and a photodiode (PD) is widely used for various applications. In general, bandwidth and quantum efficiency are important figures of merit for high-speed PDs, though constraints exist due to the tradeoff between these characteristics [4]. In addition, the high-output capability of a PD has also become very important for making full use of the superior features of optical components, such as wide bandwidth and wide-frequency tunability. This is because the combination of a high-output PD and a broadband optical fiber amplifier (OFA) can eliminate postamplification electronics and thus extend the bandwidth of the entire system [5]. This new photoreceiver configuration is also superior in terms of system simplicity and input sensitivity [6]. However, in a conventional pin PD, there are inherent tradeoffs between the output power and the other important characteristics mentioned above [4], [7].

To overcome these problems, we have developed a novel photodiode named the unitraveling-carrier photodiode (UTC-PD) [8]. The UTC-PD provides a high 3-dB down bandwidth $(f_{3\ \mathrm{dB}})$ and a high-saturation output power simultaneously because it has a unique operation mode where only electrons are the active carriers traveling through the junction depletion later [9]–[11]. To date, an $f_{3\ \mathrm{dB}}$ of 310 GHz [12] and an output power of more than 20 mW at 100 GHz [13] have been demonstrated. This superior performance of the UTC-PD can drastically expand its application area, not only as a high-speed photoreceiver in communications systems [6], [14], [15] but also as a high-power photonic millimeter and submillimeter-wave generator both in wireless communications and high-frequency measurements [16]–[19]. In addition, monolithic integrations of UTC-PDs with various elements, such as electron devices [20], optical devices [21], and passive components, including a resonating matching circuit [22] and a planar antenna [23], [24], are also promising, since the effective fusion of the excellent features of each element can lead to novel functions with superior performance that exceeds the limits of conventional electronics and optoelectronic integrated circuit (OEIC) technologies.

In this paper, the operation mode, basic device performance, and applications of the UTC-PD are described. First, we discuss how its operation mode differs from that of the pin PD. Next, some typical characteristics of the UTC-PD, such as bandwidth, output current, operating voltage, efficiency, and reliability are presented. Then, as digital applications, high-speed photoreceivers and an integrated optical gate for ultrafast signal processing in broadband optical communications systems are described. Finally, as analog applications, a high-power millimeter-wave generator for high-frequency measurement systems and millimeter-wave fiber radio communications systems are presented.

Manuscript received March 31, 2004; revised May 20, 2004.

H. Ito, S. Kodama, Y. Muramoto, and T. Furuta are with NTT Photonics Laboratories, NTT Corporation, Kanagawa 243-0198, Japan.

T. Nagatsuma is with NTT Microsystem Integration Laboratories, NTT Corporation, Kanagawa 243-0198, Japan.

T. Ishibashi is with NTT Electronics Corporation, Tokyo 194-0004, Japan.

Digital Object Identifier 10.1109/JSTQE.2004.833883

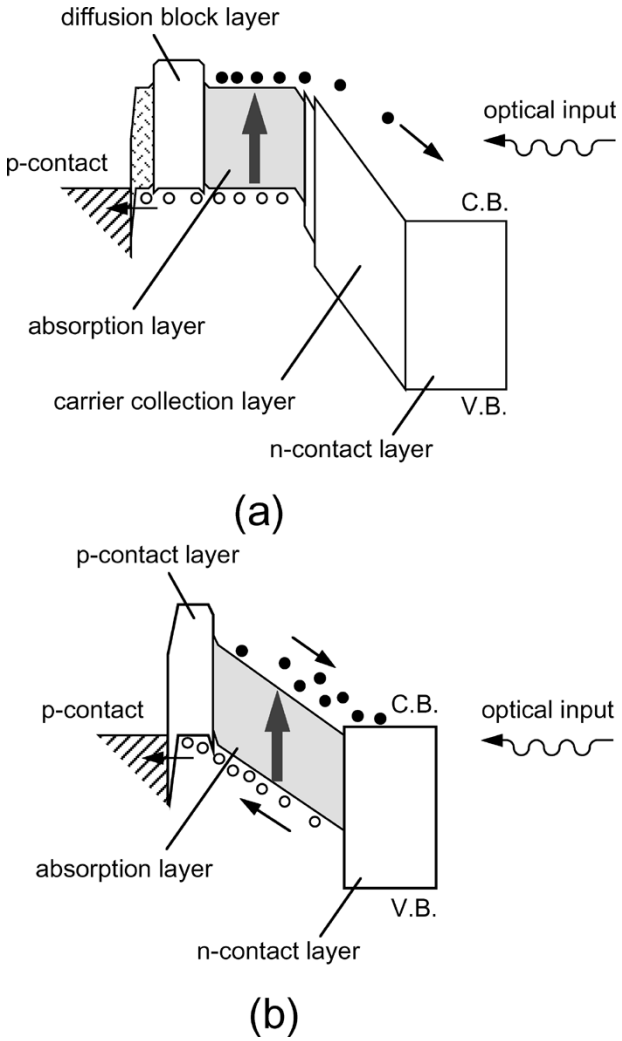

Fig. 1. Band diagram of (a) UTC-PD and (b) pin PD.

II. Operation of the UTC-PD

Band diagrams of the UTC-PD and pin PD are schematically shown in Fig. 1(a) and (b). The active part of the UTC-PD consists of a neutral (p-type) narrow-gap light absorption layer and an undoped (or a lightly n-type doped) wide-gap (depleted) carrier-collection layer. The photo-generated minority electrons in the neutral absorption layer diffuse (and/or drift) into the depleted collection layer. Here, introducing a quasi-field into the absorption layer by means of the band-gap grading and/or doping grading is very effective in reducing electron traveling time [10]. On the other hand, because the absorption layer is quasi-neutral, photogenerated majority holes respond very fast within the dielectric relaxation time by their collective motion. Therefore, the photoresponse of a UTC-PD is determined only by the electron transport in the whole structure. This is an essential difference from the conventional pin PD [Fig. 1(b)], in which both electrons and holes contribute to the response current and the low-velocity hole-transport determines the total performance [7]. In addition, in the UTC-PD structure, we can effectively use the velocity overshoot of electrons [25] in the depletion layer. This qualitatively different operation mode of the UTC-PD provides several advantages.

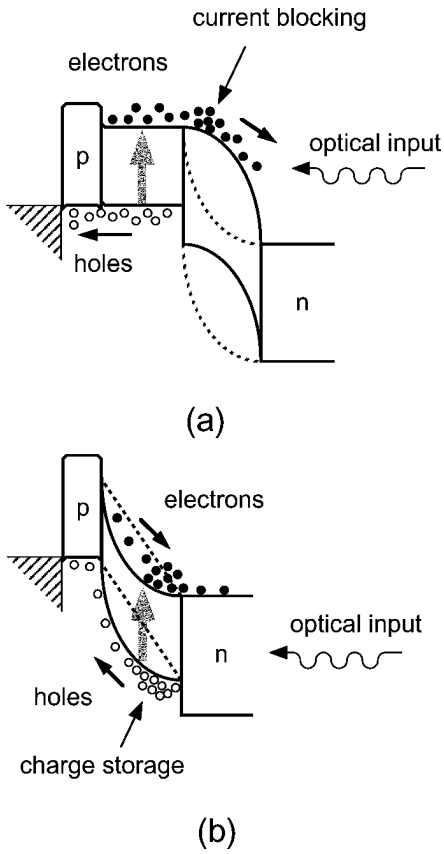

Fig. 2. Modified band diagram of (a) UTC-PD and (b) pin PD at high-optical input.

One advantage is higher device operation speed because of the order of magnitude higher electron velocity in the depletion layer compared to hole velocity. In an appropriate UTC-PD structure with a moderate absorption layer thickness, electron diffusion time mainly determines the operation speed. In general, diffusion velocity is considered to be smaller than the drift velocity. However, the electron diffusion velocity in the InGaAs absorption layer can be very large for a relatively thin absorption layer due to the uniquely large minority mobility of electrons in p-InGaAs [26], even if the absorption layer has a uniform band gap and doping structure. In addition, we can independently design the depletion layer and the absorption layer thicknesses in the UTC-PD structure. Thus, a very thin absorption layer can be used to attain an extremely high $f_{3\ \mathrm{dB}}$ without sacrificing the CR charging time. This is also an important advantage over the pin PD, in which the CR charging time becomes significantly larger when the absorption layer thickness is excessively reduced to decrease the carrier transit time [4].

Another advantage is the higher output saturation current due to much less space charge effect in the depletion layer, which also results from the high electron velocity in the depletion layer. In the conventional pin PD, the band profile is modified under a high-excitation condition because photogenerated carriers are stored in the absorption layer as shown in Fig. 2(b). The decreased electric field drastically reduces the carrier velocity, enhances the charge storage, and eventually results in output current saturation. Although the situation is similar in the

UTC-PD [Fig. 2(a)], the space charge consists of only electrons whose velocity at overshoot is much higher than that of holes even for the decreased electric field. Therefore, the output does not saturate until the current density becomes an order of magnitude higher than that for the pin PD.

An important point here is that the velocity reduction of holes (output saturation in pin PD) starts to occur even when the current density is relatively low. This is in contrast to the UTC-PD, where the prominent velocity reduction of electrons (output saturation) does not occur until the electric field becomes much smaller [25]. Therefore, the linearity range of the UTC-PD is much wider than that of conventional pin PD. Another important point is that the high speed with high-saturation output is maintained at a low (or even at zero) bias voltage [27], because the high electron velocity in the depletion layer can be maintained at a relatively low electric field [25] or even with the built-in field of the pn junction. This makes the high-speed operation of the UTC-PD possible without applying any bias voltage [27]. A smaller operation voltage is advantageous in many ways; it reduces power consumption, simplifies heat sinking, reduces biasing circuit cost, and improves reliability.

III. Device Fabrication and Characterization

The InP–InGaAs UTC-PD epilayers are grown on a (100) oriented semi-insulating (S.I.) InP substrate by low-pressure metal–organic chemical vapor deposition (MOCVD). The p-type and n-type dopants are usually C and Si, respectively. The absorption layer consists of p-InGaAs, thin p^+InGaAs, and thin undoped InGaAs, and the collection layer consists of thin undoped InGaAsP, thin undoped InP, thin n^+InP, and lightly n-doped or undoped InP. Here, the p-InGaAs absorption layer is moderately doped (typically from 1 to $10\times10^{17}/\mathrm{cm}^3$) so as to obtain the benefit from the self-induced field (self-bias effect) in the absorption layer [9], [28]. In order to suppress current blocking at the absorption/collection layer interface, we use a step-graded band-gap profile, inserting an InGaAsP (typical band-gap energy of about 1 eV) layer between the InGaAs absorption and InP collection layers. For characterizing the high-speed performance of devices, double-mesa structure devices are fabricated by wet chemical etching and liftoff processes. Unless otherwise mentioned, back-illuminated configuration is employed. Each device is then integrated with 50-Ω coplanar lines on the S.I. InP substrate. The backside of the substrate is mirror-polished and antireflection coated after the device fabrication.

The responsivity measurement is usually done at $\lambda = 1.55-\mu$m in a device with an area of 2500 $\mu\mathrm{m}^2$. The pulse photoresponse was measured by a pump-probe electro-optic sampling (EOS) technique [29] with a 1.55-μm incident pulse (a full width at a half maximum (FWHM) of 280 or 400 fs; the repetition rate is 30 or 100 MHz) using an external CdTe probe chip. The RF output power measurement was performed by using an RF optical source, such as a laser diode with an external modulator, a semiconductor mode-locked laser, or optical heterodyning with two wavelength tunable lasers, and using a detector, such as a Schottky diode, a power meter, or an InSb hot-electron bolometer.

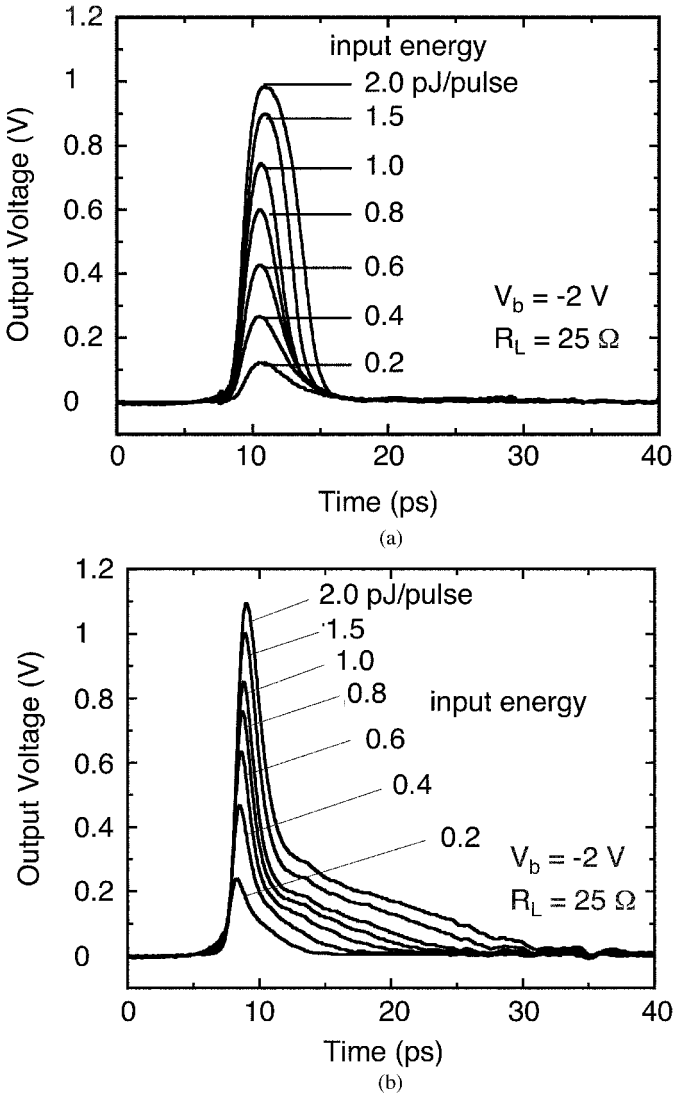

Fig. 3. Pulse photoresponse of (a) UTC-PD and (b) pin PD.

IV. Device Characteristics

A. Basic Photoresponse

Fig. 3(a) and (b) shows output waveforms of the pulse photoresponse of a UTC-PD and a pin PD [7] measured using the EOS technique. For the measurement, the input energy was changed from 0.2 to 2.0 pJ/pulse and bias voltage was fixed at -2 V. In order to make a reasonable comparison, both devices were designed to have the same junction capacitance and the load resistance (25 Ω).

In the UTC-PD, the output peak current increases linearly with increasing input energy, and the waveform does not significantly change until it reaches the saturation point. After the saturation occurs, the pulsewidth increases gradually. However, even at this stage, the fall time of the waveform does not obviously increase. The output current saturation is caused by the space-charge-induced modification of the electric field in the collection layer as mentioned in the previous section. Thus, the fast fall time even in the saturation region is attributed to the fast response of electrons accumulated in the depletion layer.

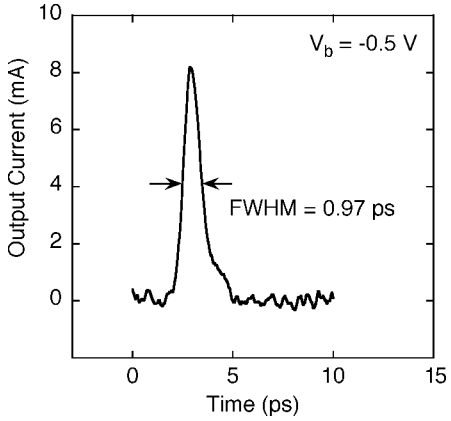

Fig. 4. Pulse photoresponse of a UTC-PD with a fast-response design.

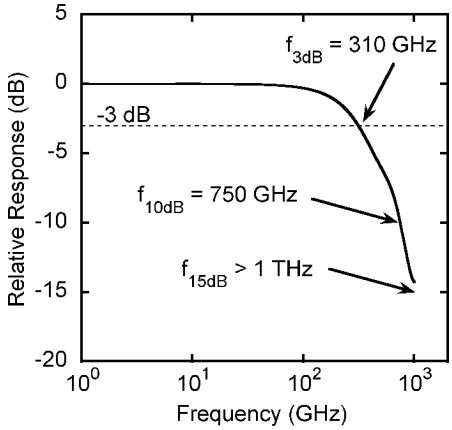

Fig. 5. Fourier transform of the waveform in Fig. 4.

On the other hand, the waveform of the pin PD is quite different and it consists of two current components. The initial sharp component (FWHM of about 1 ps) is attributed to electron transport, and the slow tail is caused by hole transport. The peak current of the electron response starts to saturate at relatively low input energy, and the pulsewidth increases gradually at the same time. In contrast, the full width of the hole response increases drastically as the input energy increases. This is due to the stronger space charge effect of holes in the depletion (absorption) layer of the pin PD. The much slower hole response compared to that of electrons produces hole accumulation and band flattening around the cathode region in the depletion layer. The reduction of the electric field in the depletion layer causes even slower hole transport, and this feedback finally results in a significant broadening of the photoresponse waveform. The broadening in turn results in severe degradation of the bandwidth and linearity of the pin PD in a high excitation condition [7].

This comparison clearly indicates that the UTC-PD is superior for obtaining wide linearity and a very high output level while maintaining a broad bandwidth.

B. Bandwidth

Fig. 4 shows the pulse photoresponse of a back-illuminated InP–InGaAs UTC-PD with a fast-response design in which absorption layer thickness is 30 nm, collection layer thickness (W_C) is 230 nm, and an absorption area (S) is 5 μm^2 [12]. The shortest pulsewidth (FWHM) of 0.97 ps was obtained at a very low bias voltage of -0.5 V. The Fourier transform of this pulse response gives an $f_{3\ \mathrm{dB}}$ of 310 GHz as shown in Fig. 5. This is the highest $f_{3\ \mathrm{dB}}$ ever reported for PDs operating at 1.55 μm. This device also exhibited a 10-dB down bandwidth of 750 GHz, and a 15-dB down bandwidth of over 1 THz. The estimated average electron velocity in the entire device is as high as 3×10^7 cm/s [12], which is about three times as large as the reported electron drift velocity of about 1×10^7 cm/s in undoped InP at a similar electric field [30]. This indicates that electron velocity overshoot is actually taking place in the depletion layer of the UTC-PD.

Fig. 6 shows the relationship between $f_{3\ \mathrm{dB}}$ and absorption layer thickness (W_A) for back-illuminated InP–InGaAs

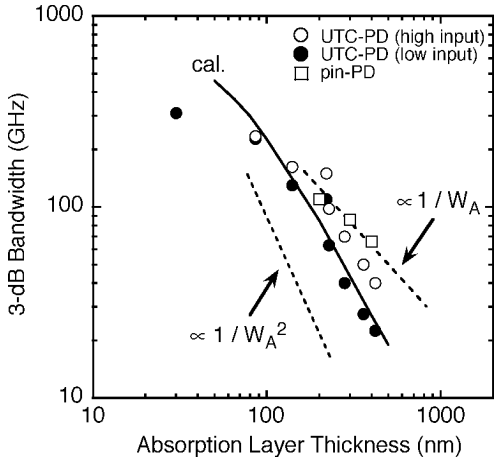

Fig. 6. Relationships between $f_{3\ \mathrm{dB}}$ and W_A for UTC-PDs and pin PDs.

UTC-PDs [31]. These data were obtained from the Fourier transform of pulse photoresponses. Data for conventional pin PDs are also shown for comparison. As shown in this figure, the $f_{3\ \mathrm{dB}}$ is proportional to $1/W_A^2$ for the UTC-PD and to $1/W_A$ for the pin PD. This difference comes from the difference in the carrier transport in the absorption layer; namely, the electron transport in the neutral absorption layer is diffusive in the UTC-PD, which is in contrast to the drift motion of both carriers in the depletion layer of the pin PD. The $f_{3\ \mathrm{dB}}$ at high optical inputs (large signal outputs) is enhanced due to the effect of the self-induced field in the absorption layer [9], [28]. (These behaviors are discussed in detail in the following sections.) As can also be seen in this figure, $f_{3\ \mathrm{dB}}$ for the UTC-PD increases monotonically with the reduction of $\mathrm{W_A}$, while there is an inevitable limit for the pin PD because the CR charging time will increase significantly with further reduction of W_A [4].

A simplified expression of the 3-dB bandwidth for the pin PD [4] is

$$f_{3\ \mathrm{dB}} \cong \frac{3.5}{2\pi\tau_{\mathrm{hole}}} \tag{1}$$

where τ_{hole} is average hole traveling time in the depletion layer $(= W_A/v_{\mathrm{hole}})$ and v_{hole} the average hole velocity. Thus, $f_{3\ \mathrm{dB}}$ is basically inversely proportional to $\mathrm{W_A}$. On the other hand, when the electron transport in the collection layer is dominant

as in the extreme case ($W_A = 0$), the 3-dB bandwidth for the UTC-PD is similarly expressed [11] as

$$f_{3\ \mathrm{dB}} \cong \frac{2.8}{2\pi\tau_{\mathrm{electron}}} \tag{2}$$

where τ_{electron} is average electron traveling time in the collection layer ($= W_C/v_{\mathrm{electron}}$) and v_{electron} the average electron velocity. Note that τ_{electron} is much smaller than τ_{hole} because electron velocity at overshoot (4×10^7 cm/s) [25] is much larger than hole drift velocity (5×10^6 cm/s) [32]. In reality, the electron diffusion time in the absorption layer dominates the total carrier transit time in the UTC-PD except in the case of a very thin absorption layer. In such a case, the 3-dB bandwidth is expressed [11] as

$$f_{3\ \mathrm{dB}} \cong \frac{1}{2}\left(\frac{W_A^2}{3D_e} + \frac{W_A}{v_{\mathrm{th}}}\right) \tag{3}$$

where D_e is the diffusion coefficient of minority electrons in p-InGaAs and v_{th} the thermionic emission velocity of electrons. This indicates that the $f_{3\ \mathrm{dB}}$ of the UTC-PD is basically inversely proportional to W_A^2 except when the absorption layer is very thin.

The solid line in Fig. 6 shows the calculated tendency for the UTC-PD, which considers contributions of both carrier transit times in absorption and collection layers. The calculation agrees well with the experimental results except for the highest $f_{3\ \mathrm{dB}}$ case, where the absorption layer is extremely thin, i.e., 30 nm. We believe this is due to the resolution limit of our experimental setup, because we have not properly accounted for factors such as the finite influence of the pulsewidth widening caused by the transmission characteristics of optical fibers, the light round-trip time in the CdTe chip, and the finite dimension of the optical probe beam on the waveguide.

C. Effect of the Self-Induced Field

The $f_{3\ \mathrm{dB}}$ enhancement at high-optical inputs (large signal outputs) results from the effect of the self-induced field in the absorption layer [9], [28]. When the intensity of the optical signal is relatively high, hole drift current prominently contributes to the total current flow, because the hole current must flow through the absorption layer to maintain the current continuity such that

$$J(x)_{\mathrm{hole}} + J(x)_{\mathrm{electron}} = \mathrm{const.} \tag{4}$$

where $J(x)_{\mathrm{hole}}$ is hole current density at position x and $J(x)_{\mathrm{electron}}$ electron current density. This hole drift current induces an electric field in the absorption layer, $E(x)_{\mathrm{ind}}$, without any external biasing signal, such that

$$E(x)_{\mathrm{ind}} \cong \frac{J(x)_{\mathrm{hole}}}{\sigma_p} \tag{5}$$

where σ_p is the conductance of the absorption layer ($= qp_0\mu_{\mathrm{hole}}$), q the electron charge, p_0 the doping level of the absorption layer, and μ_{hole} the majority hole mobility in the absorption layer.

This automatically induced field in the absorption layer accelerates the photogenerated minority electrons in the absorption layer. Thus, when the operation current is above a certain level, the electron transport is regarded to be drift rather than diffusion. Such a phenomenon enhances the $f_{3\ \mathrm{dB}}$ of the UTC-PD in a high-excitation condition. $J(x)_{\mathrm{hole}}$ is zero at the absorption/collection layer interface and linearly increases (under uniform carrier generation) toward the p-contact layer side up to the diode operation photocurrent density J_{op}. Thus, the maximum induced field $E(0)_{\mathrm{ind}}$ does not depend on the absorption layer thickness, while the diffusion velocity decreases in reverse proportion to W_A^2. This implies that the benefit of this self-induced field is prominent when the absorption layer is relatively thick.

The total potential drop in the absorption layer $\Delta\phi_{\mathrm{ind}}$ is then expressed as

$$\Delta\phi_{\mathrm{ind}} \cong \frac{J_{op}W_A}{2qp_0\mu_{\mathrm{hole}}}. \tag{6}$$

This equation indicates that the benefit of the self-induced field is stronger for smaller p_0 and proportional to the photocurrent, I_p ($= J_{\mathrm{op}}\times S$). For example, when $p_0 = 4\times10^{17}$ /cm^3, $\mu_{\mathrm{hole}} =$ 130 cm^2/Vs, and $J_{\mathrm{op}} = 100$ kA/cm^2 ($I_p = 50$ mA for $S =$ 50 μm^2), $E(0)_{\mathrm{ind}}$ is calculated to be 12 kV/cm, which results in a drift velocity of 7.4×10^7 cm/s with a minority electron mobility of 6200 cm^2/Vs. This is much higher than the pure diffusion velocity of 1.6×10^7 cm/s for $W_A = 300$ nm (for example), which can well explain the observed enhancement of $f_{3\ \mathrm{dB}}$ in Fig. 6.

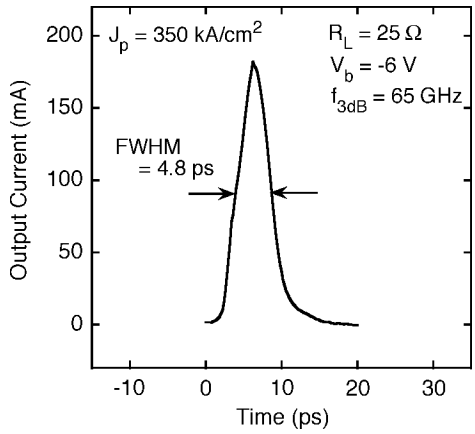

Fig. 7. Pulse photoresponse of a UTC-PD with a high-output design.

D. High Peak Output Current

Fig. 7 shows the pulse photoresponse of a UTC-PD with a high-output design in a very high excitation condition [31]. Here, the absorption area was 52 μm^2, W_A was 220 nm, load resistance was 25 Ω, bias voltage was -6 V, and optical input energy was 8.7 pJ/pulse. The peak photocurrent reaches 184 mA (corresponding to a current density of 350 kA/cm^2), while the FWHM stays at 4.8 ps. The Fourier transform of this pulse response resulted in an $f_{3\ \mathrm{dB}}$ of 65 GHz. This peak photocurrent is about an order of magnitude larger than that obtainable with conventional pin PDs with similar bandwidths. We also characterized a back-illuminated UTC-PD with W_A of 86 nm, W_C of 230 nm, and S of 13 μm^2 [31], [33]. The $f_{3\ \mathrm{dB}}$ decreased with increasing input pulse energy or increasing reverse bias voltage due to the space charge effect or the shift of electric field from the optimum velocity-overshoot condition. Nevertheless, a high

peak output current (I_p) of 30 mA (230 kA/cm^2) was obtained with an $f_{3\ \mathrm{dB}}$ of 185 GHz. These results clearly indicate the superior high-output capability of the UTC-PD.

For a high-output current, some parameters must be optimized. Making the absorption area larger and the collection layer thinner can increase the maximum output current, but doing so deteriorates the CR-time limited bandwidth. Higher collection layer doping is also preferable; however, it may cause smaller junction breakdown voltage. The device configuration for better heat sinking is also a concern, because the maximum operation current may be limited by thermal destruction. In this regard, the UTC-PD structure is advantageous, since the InP collection layer, on which the high electric field is applied, has a much larger thermal conductivity [34] than that of an InGaAs absorption layer [34], on which the high electric field is applied in the pin-PD structure. The output saturation behavior of the UTC-PD for the continuous optical signal (either pseudorandom bit sequence of sinusoidal) input is discussed in the following sections.

E. Zero-Biased Operation

Eliminating the electric power supply is practically important for technologies such as microwave photonics and for portable measurement instruments because it makes systems simpler, smaller, lighter, and less expensive. Eliminating conductive cables [35] is also advantageous because it matches systems immune to electrical surge and ensures the electromagnetic field distribution is not disturbed. For such a requirement, the UTC-PD is also promising, since the build-in field in the pn junction depletion region is sufficient for maintaining its high-speed and high-output capabilities.

We measured the pulse photoresponse of a UTC-PD with W_A of 30 nm and S of 5 μm^2 at zero bias condition [31]. Despite the fact that no bias voltage was applied, the UTC-PD exhibited a very short pulse response with a width (FWHM) of 1.22 ps. Its Fourier transform (after a deconvolution) resulted in an $f_{3\ \mathrm{dB}}$ of 230 GHz. This excellent performance arises from the superior transport characteristics of electrons at the relatively low electric field in the InP depletion layer. The output peak current was as high as about 7 mA, which is comparable to the typical output peak current in conventional 50-GHz-class high-speed pin PDs operated at a higher bias voltage, while the obtained $f_{3\ \mathrm{dB}}$ is much higher than the record $f_{3\ \mathrm{dB}}$ of conventional pin PDs (110 GHz) [36], [37]. For example, maximum RF output powers of -5.9 dBm at 59.4 GHz [38] and -2.4 dBm at 100 GHz [13] have been obtained from UTC-PDs without applying bias voltage.

We have also proposed a novel UTC-PD configuration for the zero-biased condition as shown in Fig. 8 [27]. This new PD features two cascade-connected UTC-PDs and an integrated 3-dB optical signal splitter. The maximum available output voltage at zero-bias operation of a single PD is restricted by the diode turn-on voltage, which is about 0.5 V for an InGaAs pn junction. In contrast, in our configuration, the photogenerated voltage of one PD is added to that of the other, so the maximum available output voltage is twice as large as that of a conventional single PD. The pulse photoresponse of this device at a bias voltage of 0 V and an input power of 0.2 pJ/pulse resulted in a pulsewidth

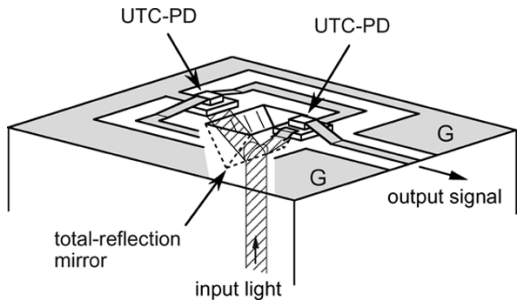

Fig. 8. Schematic drawing of the cascade-twin UTC-PD.

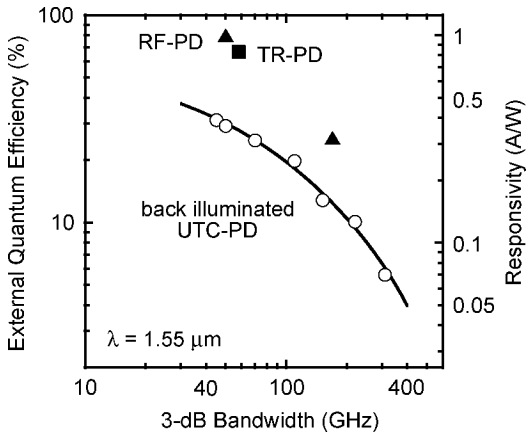

Fig. 9. Relationship between 3-dB bandwidth and efficiency for several types of UTC-PDs.

(FWHM) of 4.3 ps. The Fourier transform of this pulse response gives a 3-dB bandwidth of 63 GHz. In pulse photoresponse measurements, large V_p of 0.75 V at an $f_{3\ \mathrm{dB}}$ of 20 GHz, 0.5 V at an $f_{3\ \mathrm{dB}}$ of 40 GHz, and 0.2 V at an $f_{3\ \mathrm{dB}}$ of 60 GHz were obtained under the zero-bias condition. We can expect RF output voltages that are higher by a factor of two (RF output powers higher by a factor of four) than those above when we use a continuous optical RF signal input (instead of a pulse signal input with a low repetition rate) because of the extended load line on both sides of the zero-bias point. These results clearly demonstrate that this novel UTC-PD structure is promising for increasing the available output voltage of a PD at zero-bias without degrading its high-speed characteristics.

F. Efficiency

Another important figure of merit is efficiency, which is directly related to absorption layer thickness. The back-illuminated configuration has certain advantages over the surface-illuminated one since it can use reflected light signal at the surface electrode to increase the efficiency. Fig. 9 shows the relationship between the 3-dB bandwidth and efficiency in the back-illuminated UTC-PDs (open circles) we have fabricated [31]. There is a tradeoff between $f_{3\ \mathrm{dB}}$ and efficiency, and these values may still be insufficient for some applications. In order to increase the efficiency without sacrificing the high-speed characteristics, several types of UTC-PDs, such as a waveguide UTC-PD (WG-PD) [39], a refracting-facet UTC-PD (RF-PD) [40], and a total-reflection UTC-PD (TR-PD) [41], have been developed.

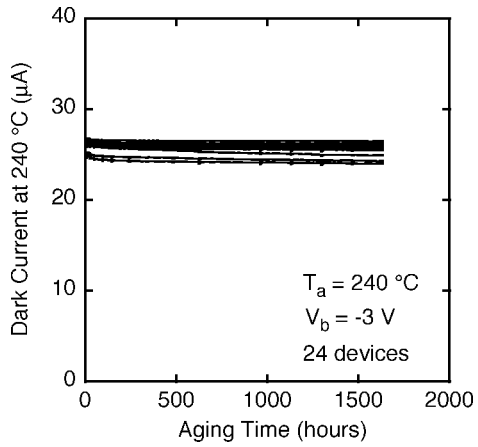

Fig. 10. Variation of dark current against aging time during the bias-temperature stress test.

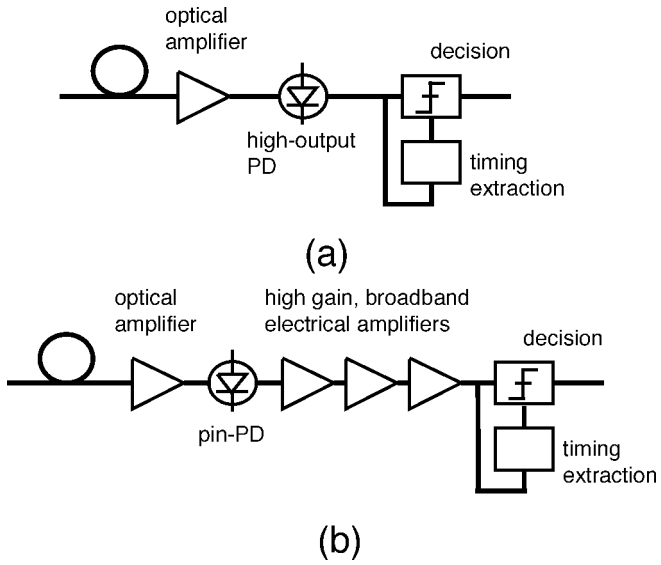

Fig. 11. Photoreceiver consisting of (a) optical preamplifier and a high-output PD and (b) one consisting of a conventional PD and electrical postamplifiers.

The RF-PD and the TR-PD utilize angled irradiation of the signal light onto the absorption layer to increase the light propagation length in the absorption layer. In order to guide the input light diagonally, the RF-PD uses the refraction of the edge-illuminated light at an angled edge, while the TR-PD employs the total-reflection of back-illuminated light at a V-grooved mirror formed adjacent to the PD. The results for a RF-PD (closed triangles) and a TR-PD (closed square) are also shown in Fig. 9. The RF-PD achieved a responsivity of 1.0 A/W with an $f_{3\ \mathrm{dB}}$ of 50 GHz [42] and 0.32 A/W with an $f_{3\ \mathrm{dB}}$ of 170 GHz, while the values are 0.83 A/W with an $f_{3\ \mathrm{dB}}$ of 58 GHz for the TR-PD. These values are more than twice as large as that obtained by the back-illuminated device.

In contrast, The WG-PD utilizes a ridge waveguide to confine the input light into the absorption region. This is advantageous for increasing efficiency with maintaining a very small carrier traveling distance. However, the edge illumination is generally regarded to be disadvantageous for high-intensity light input because the highest absorption (photo-generated carrier density) near the edge surface may cause a catastrophic degradation. One way to relax this constraint is to employ a velocity-matched distributed PD structure [43]. We thus investigated a periodic traveling-wave UTC-PD structure and found that a careful design of the device configuration can attain proper velocity matching in the distributed structure with a high $f_{3\ \mathrm{dB}}$ of 115 GHz [44].

G. Reliability

Reliability is also a very important issue for practical applications. We performed bias-temperature stress test of UTC-PDs designed for 40 Gb/s optical communications systems [45]. Fig. 10 shows the variation of the dark currents for 24 devices monitored during the aging test at 240 °C with a bias voltage of −3 V. The PD has a responsivity of 0.8 A/W and an $f_{3\ \mathrm{dB}}$ of 47 GHz at a photocurrent of 10 mA. The change in the dark current was very small over 1600 h, and no failure was observed. Taking the results of additional tests at temperatures of 170 and 200 °C with a total device number of 74 into account, we estimated the failure rate as smaller than 42 FIT at 25 °C. Here, the random failure mode with an activation energy of 0.35 eV was assumed [according to the Telcordia Generic Reliability Assurance Requirements (GR-468-CORE)]. This failure rate satisfies the general requirement (less than 100 FIT) for practical system applications.

Because the UTC-PD is typically operated at a high current level, we also have to look at the long-term stability under an optical input stress. Thus, we also tested devices at a photocurrent of 20 mA with a bias voltage of −2 V at elevated temperature of 85 °C. This temperature is the upper limit for optical parts used in pig-tailed modules. The dark current stayed at a very low level (less than ten times the initial value and less than 1 μA) for more than 7000 h. These results indicate that UTC-PD is sufficiently reliable for practical system applications.

V. Digital Applications

A. Photoreceiver

A typical digital application of the UTC-PD is a photoreceiver for ultra-high bit-rate communications systems. Fig. 11(a) and (b) shows configurations of a photoreceiver with an optical preamplifier and a high-output PD and a conventional one with electrical post amplifiers. The high output capability of the UTC-PD in combination with an OFA [Fig. 11(a)] makes it possible to drive the decision circuit directly without post electrical amplifiers [5]. Such a configuration provides several advantages, such as wider bandwidth, a simpler system, and better sensitivity [6], [15] and is considered to be suitable for systems operating at 40 Gb/s or higher. For example, we have demonstrated high-output photoreceiver operations at 80 Gb/s [14]. The generated nonreturn-to-zero (NRZ) pseudorandom bit sequence (PRBS) signal at 80 Gb/s was transmitted through an 89-km optical fiber as one channel of 1.04 Tb/s WDM signal and amplified in front of the PD using an OFA. The eye opening was clear with a peak-to-peak voltage of 0.8 V, which is sufficient for directly driving the digital circuit after the PD. Error-free operation with an input sensitivity of less

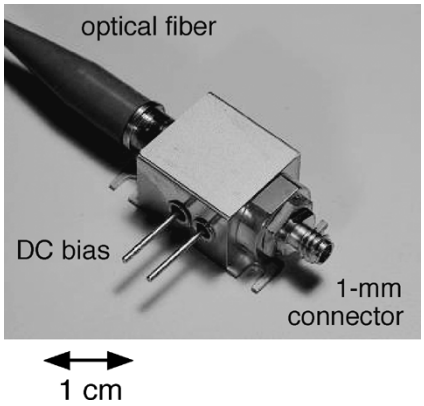

Fig. 12. Photograph of the UTC-PD module with a 1-mm coaxial connector.

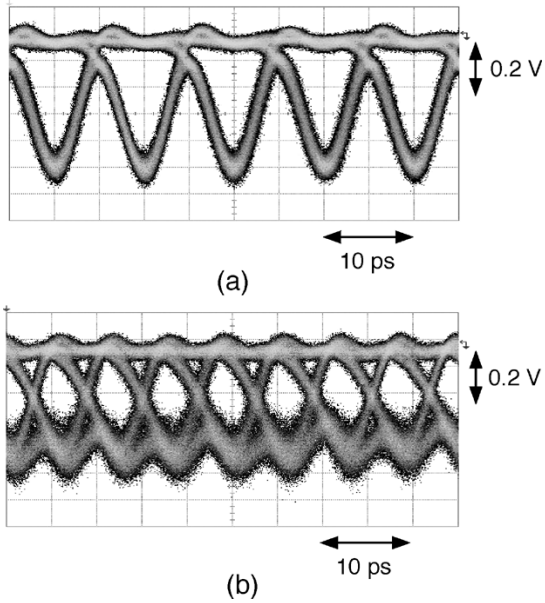

Fig. 13. Eye diagrams for (a) 100- and (b) 160-Gb/s PRBS optical signal inputs received using the fabricated 1-mm connector UTC-PD module.

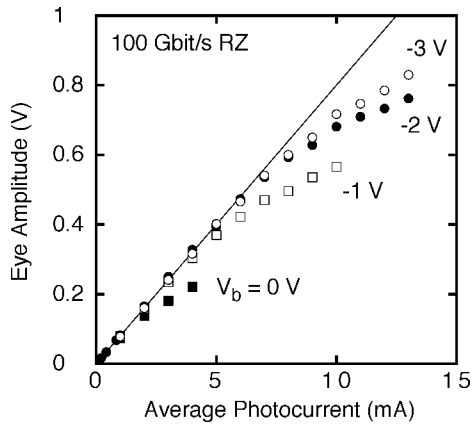

Fig. 14. Eye amplitude against average photocurrent at 100 Gb/s signal input for several bias voltages.

than −17 dBm was also confirmed for all 10-Gb/s time slots ($8\times13=104$ slots).

Although even faster operation is possible, the electrical coaxial connection in the current hybrid assembly scheme (V-connector technology) limits the operation at frequencies higher than 75 GHz. One way to overcome this limitation is to use a 1-mm connector, which has a bandwidth of 110 GHz. Fig. 12 shows a photograph of fabricated UTC-PD module with a 1-mm connector [46]. The UTC-PD chip integrates a biasing circuit consisting of a capacitor and a matched resistor (50 Ω) and was electrically connected with the 1-mm connector by means of a microstrip-line fabricated with quartz substrate. Then, the PD was optically coupled with an optical fiber by using a two-lens system. The optical parts were fixed onto the package using a YAG laser welder. The RF response of this module was evaluated my measuring the frequency characteristics of the output power at frequencies of up to 110 GHz, and it was found that the 3-dB bandwidth was about 80 GHz [46].

Fig. 13(a) and (b) shows the output waveforms of the fabricated UTC-PD module for 100- and 160-Gb/s return-to-zero (RZ) signal [47] observed with an 80-GHz-bandwidth sampling oscilloscope (with Agilent 86 116B). Clear eye openings with very high eye amplitudes of 0.5 V at 100 Gb/s and 0.3 V at 160 Gb/s were obtained. To our knowledge, these are the first eye-diagram observations from PD modules at bit rates of over 100 Gb/s. For the 160-Gb/s case, degradations in the eye amplitude and in the waveform (to be NRZ-like), including a signal phase delay, are observed. These degradations are attributed to the insufficient bandwidths of the fabricated module (80 GHz) and the sampling head (80 GHz).

Fig. 14 shows the eye amplitude against the photocurrent for several bias voltages at 100 Gb/s. The eye amplitude increases linearly with increasing photocurrent until it saturates. The linearity is maintained for eye amplitude of over 0.5 V, and the maximum value exceeds 0.8 V, which is more than an order of magnitude larger than that obtained by a conventional pin-PD module operating at 80 Gb/s [48], [49]. It is worth mentioning that this module could be operated at zero bias voltage with a linear output voltage of over 100 mV with a clear eye opening.

B. Ultrafast Optical Gate

At bit rates of over 100 Gb/s, electronics-based technology must be supplemented with photonics-based technology. In this regard, the UTC-PD can be used as an optical driver to overcome the speed limitation of electronic circuits.

We have developed a novel O/E/O-type optical gate, named the PD-EAM [21], [50], [51], which monolithically integrates a UTC-PD and an electroabsorption modulator having a traveling wave electrode (TW-EAM). Fig. 15 is a schematic drawing of the PD-EAM. In the PD-EAM, the anode of a UTC-PD is directly connected to the anode of the TW-EAM using a thin-film microstrip line (MSL). Such a configuration is possible because the UTC-PD can supply sufficient voltage to drive the EAM. The other side of the TW-EAM anode is connected to the terminal resistor (R_T) using the MSL. With an optical input (gate signal) to the UTC-PD, the generated photocurrent provides a positive bias voltage to the TW-EAM, making the waveguide transparent for the input optical signal. Thus, this integrated device functions as a transmission-type optical gate. By simply changing the electrical connection in the above configuration, we can also fabricate an inverter-type optical gate. Because there is no electrical signal interface outside of the chip, the PD-EAM

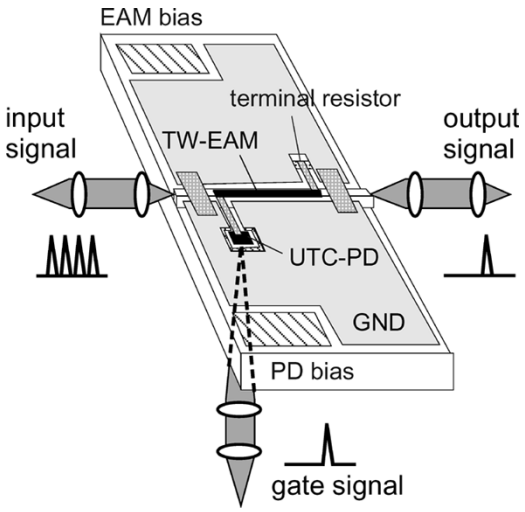

Fig. 15. Schematic drawing of a PD-EAM optical gate.

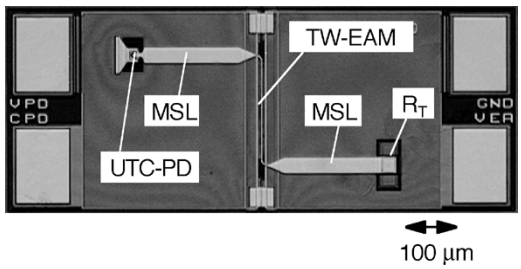

Fig. 16. Micrograph of the fabricated PD-EAM optical gate.

is free from the 50-Ω impedance-matching restriction. Thus, we used a characteristic impedance of 15 Ω (MSL, TW-EAM, and terminal resistor) to relax the influence of the CR time constant.

Fig. 16 shows a micrograph of the fabricated PD-EAM. All elements mentioned above and two bias capacitors are integrated in a chip having an area of 1×0.4 mm^2. The active region of the TW-EAM, which employs InAlGaAs–InAlAs multiple-quantum-wells, is 200-mm long, and the UTC-PD has a 3-dB bandwidth of around 160 GHz. The input signal comes from the upper edge of the device, and the gate signal to the UTC-PD comes from the backside of the chip. Using this PD-EAM, demultiplexing operation for a PRBS signal at a bit rate of 320 Gb/s was investigated [51]. The 320-Gb/s signal was generated by optically multiplexing a 10 Gb/s PRBS signals.

Fig. 17(a) and (b) shows cross-correlation traces of the input and output (demultiplexed) data signals, respectively. The input data signal has a period of ∼3.1 ps, corresponding to a data rate of 320 Gb/s. As shown in Fig. 17(b), the input signal is clearly demultiplexed by properly adjusting the timing between the input data signal and the clock (gate) signal. The on/off ratio of the demultiplexed signal is larger than 14 dB for the adjacent channels before and after the on-channel and larger than 28 dB for the furthest channel between two on-channels at optimum conditions.

Fig. 18 shows the measured bit-error rate (BER) for the 320 to10-Gb/s DEMUX together with the result for 160-Gb/s data input. Error-free operation for 320-Gb/s DEMUX was achieved with a receiver sensitivity of −18 dBm at a BER of 10^{-9}. This is the highest bit rate ever achieved for error-free operation using

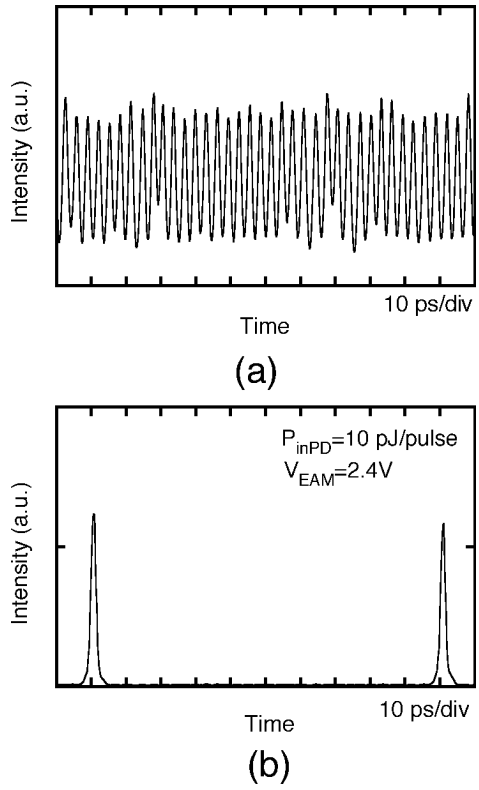

Fig. 17. Input data signal at (a) 320 Gb/s and (b) output (demultiplexed) data signals at 10 Gb/s.

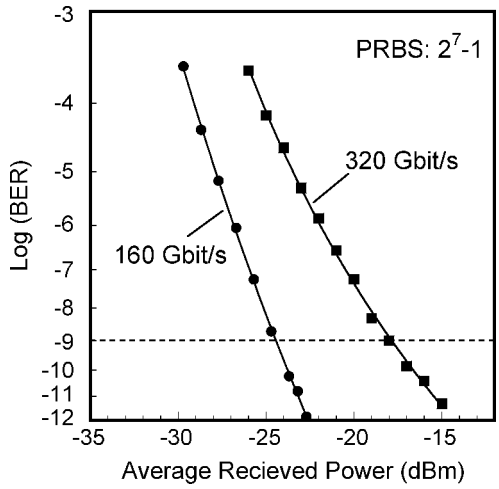

Fig. 18. BERs for the 160- and 320-Gb/s DEMUX.

an O/E/O-type optical gate. The sensitivity was obtained for a receiver that includes a demultiplexer with 320-Gb/s data input. Thus, the value for the demultiplexed 10-Gb/s data should actually be 15 dB lower than the one obtained.

We have also demonstrated ultrafast operations of the PD-EAM, including DEMUX operation for a pulse stream corresponding to a bit rate of 500 Gb/s [52], error-free full-rate retiming operation at 100 Gb/s with a timing margin of 2.2 ps [53], and optical sampling at 80 Gb/s [54]. The PD-EAM can also be used as a wavelength converter in high-bit-rate communications systems [55]. These results offer a clear demonstration that the excellent high-speed and high-output

characteristics of the UTC-PD can open up a new class of integrated devices, which can be operated at speeds beyond those possible with conventional OEIC technology.

C. Optoelectronic Integrated Circuit

The integration of optical and electrical devices is a traditional way to create novel functions and to improve device performance. The UTC-PD is especially advantageous here because it can eliminate speed-limiting electrical amplifiers and thus extend circuit bandwidth. There are several promising combinations for such direct-drive-type integration. The monolithic integration of a UTC-PD with an electrical circuit can realize high-speed digital OEICs for operation at 40 Gb/s or above [20], [56], [57]. An error-free photoreceiver operation at 40 Gb/s with a sensitivity of −27.5 dBm was achieved with an optoelectronic decision circuit that integrates a UTC-PD and a HEMT circuit (with 172 active electron devices). An optical clock divide-by-two OEIC has also been proposed and operation at 75 GHz was demonstrated [58].

The monolithic integration of a UTC-PD with ultrafast resonant tunneling diodes has been applied to an optoelectronic demultiplexer [59] and a delayed flip–flop circuit [60], [61], both of which operate at up to 80 Gb/s, a decision circuit operating at 40 Gb/s [62], and an optoelectronic clock recovery circuit operating at 46.2 Gb/s [63], [64]. These novel circuits are promising for realizing high-speed low-power optoelectronic logic gates.

VI. Analog Applications

Photonic generation of millimeter and submillimeter wave signals is a promising technique because it provides several advantages, such as an extremely wide bandwidth afforded by the characteristics of optical components, and can use low-loss fibers for transmission of very high-frequency signals. This technology can be used for various applications, including fiber-radio wireless communications systems [2], high-speed measurement systems [3], [18], [65], [66], millimeter-wave sensing and imaging systems [19], [67], [68], and a local signal supply for radio telescopes [69]. The use of a photodiode that has high-output power as well as superior high-frequency characteristics can eliminate the costly postamplification circuit and thus simplify the system configuration.

A. High-Power Millimeter- and Submillimeter-Wave Generation

To attain a high-output power level at frequencies above 100 GHz without having a significant increase of the input optical power, the implementation of additional methods to compensate for factors that restrict device performance is effective. This is because, at higher frequencies, output power decreases due to the intrinsic carrier traveling time and CR time constant limitations become significant. Considering narrow-band applications, the use of a resonating matching circuit to overcome the CR time constant limitations is a promising way to improve efficiency at desired frequencies [13].

Fig. 19 is a micrograph of a fabricated matching-circuit-integrated UTC-PD [13], [22], [70] designed for operation at 100 GHz. This device integrates a UTC-PD and a short-stub matching circuit consisting of a CPW and a MIM capacitor. This matching circuit improves the output power by compensating for the imaginary part of the internal impedance in the UTC-PD at a designed frequency.

Fig. 20 shows the relationship between the millimeter-wave output power ($P_{\rm out}$) and the diode photocurrent for this device at 100 GHz. Here, an actively mode-locked semiconductor laser was used as the optical signal source ($\lambda = 1.55\ \mu$m). As seen in this figure, a wide linearity is maintained up to a high millimeter-wave output power of over 10 mW at a bias voltage of −3 V. Such a wide linearity range is important for analog applications. The maximum output power was increased by increasing the reverse bias voltage from −1 to −3 V. The highest output power was 20.8 mW at a photocurrent of 25 mA [13]. To our knowledge, this is the highest output power ever directly generated from a PD at frequencies above the millimeter-wave range and is about two orders of magnitude larger than that obtained by a conventional pin PD [71]. The efficiency of conversion from the optical signal to the millimeter-wave power in the linear region is almost the same regardless of the bias voltage. This indicates that the UTC-PD has sufficient bandwidth for operation at 100 GHz even at a bias voltage of −1 V.

Fig. 21 summarizes the reported maximum RF output powers against the operation frequency for UTC-PDs [13], [38], [72]–[77] and conventional pin PDs [71], [78]–[80]. The difference between the two types of devices becomes larger in the millimeter-wave range, and the output power of the UTC-PDs becomes about two orders of magnitude larger at frequencies above 50 GHz. Such a large difference in the output power at higher frequencies is attributed to the difference in the space charge effect between these devices. These results clearly demonstrate that the UTC-PD can provide high-power millimeter-wave signals without electrical power amplifiers.

The optical input power $P_{\rm op}$ is related to the output RF (electrical) power $P_{\rm RF}$ as follows:

$$P_{\rm RF} = \frac{R_L r^2 P_{\rm op}^2 M B L}{2} \tag{7}$$

where R_L is load resistance, r responsivity, M a factor related to an optical modulation index, B a factor related to a PD bandwidth, and L a factor related to optical and electrical losses. When the RF modulated optical signal is a pulse, like one having a narrower pulsewidth than a sinusoidal one, the optical modulation index can be larger than 100%. This results in a larger fundamental frequency component than that in a sinusoidal signal for a fixed average optical power. If we assume the pulse has a Gaussian profile, M is expressed [81] as

$$M = 4exp\left(-\frac{\pi^2\tau^2 f_0^2}{2ln2}\right) \tag{8}$$

where τ is a pulsewidth (FWHM) and f_0 the fundamental frequency. This equation indicates that the maximum output power for a fixed average optical input power can be increased by a factor of four when we can use a very short pulse signal. The bandwidth of the photodiode also has a strong influence on the

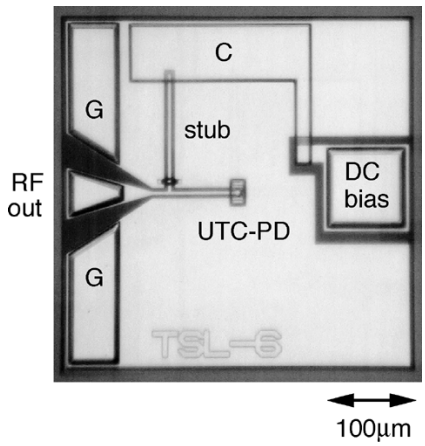

Fig. 19. Micrograph of a matching-circuit-integrated UTC-PD.

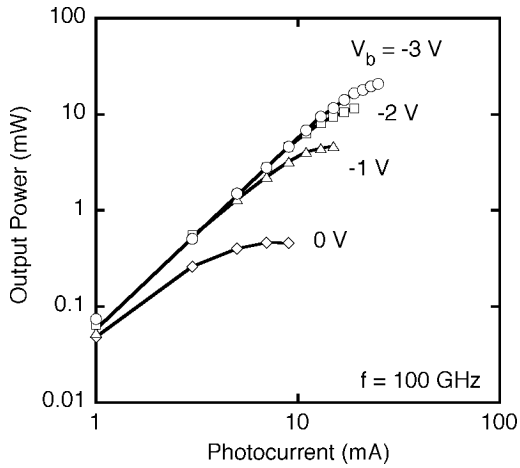

Fig. 20. Relationship between $P_{\rm out}$ and diode photocurrent at 100 GHz.

available output power. The relative output power for a wide-band-type photodiode is expressed as

$$B = \frac{1}{\left(\left(1+\left(\frac{f}{BW_{\rm CR}}\right)^2\right)\left(1+\left(\frac{f}{BW_{\rm TR}}\right)^2\right)\right)} \tag{9}$$

where f is frequency, $BW_{\rm CR}$ the CR time constant limited bandwidth $(= 1/2\pi CR)$, and $BW_{\rm TR}$ the carrier transit time limited bandwidth. We also have to carefully consider various losses, such as optical coupling loss, optical absorption, optical reflection, dielectric loss, conductor loss, and radiation loss. Looking at the results in Fig. 20 again, we see that the output power at 10 mA is 5.6 mW at 100 GHz. Taking (7)–(9) into consideration, ideal output power with a sinusoidal optical input was calculated to be 3.0 mW, assuming an overall PD bandwidth of 120 GHz. The experimental result is obviously larger than this calculation, indicating that the use of short pulse (1.5 ps) is effective for improving the output power from a PD at a constant average photocurrent. Typically, such a signal can be generated by using a mode-locked laser [82] and soliton compression [83].

The saturation of the output power is attributed to two mechanisms: the shift of the operating point to the lower reverse bias voltage and the space-charge effect in the collection layer. At the high-output power condition, the operating point shifts considerably to the lower reverse bias voltage. And, basically, the space charge effect increases with increasing photocurrent. The shift reduces the electric field in the depletion layer and thus enhances the space charge effect. The decreased reverse bias voltage also reduces the bandwidth of the UTC-PD because the junction capacitance is increased and the electric field in the depletion region is reduced. The effect of both mechanisms can be relaxed by increasing the reverse bias voltage.

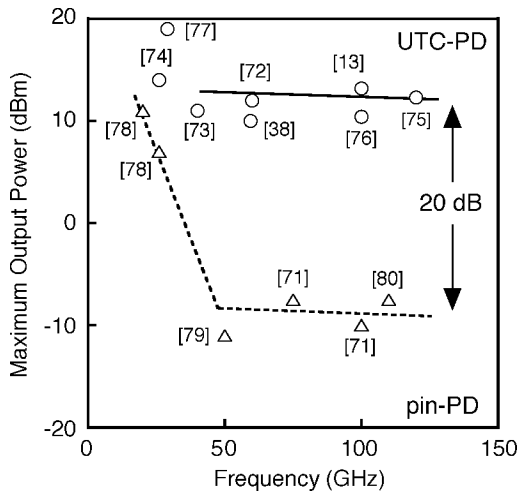

Fig. 21. Comparison of reported millimeter-wave output power against the operation frequency for UTC-PDs and pin PDs. Circles are for UTC-PDs and triangles for pin PDs. Numbers in the figure correspond to the references.

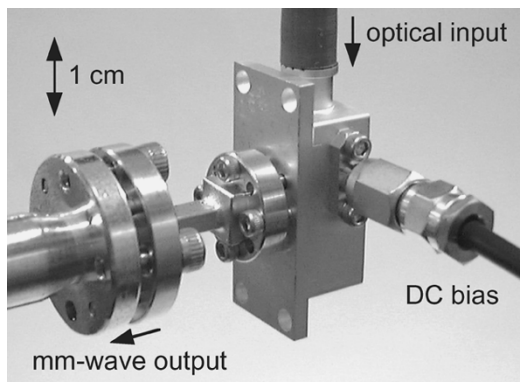

Fig. 22. Photograph of the UTC-PD module connected to a WR-8 waveguide.

B. Signal Source for Measurement Systems

The UTC-PD is advantageous for generating high-frequency and very short electrical pulse signals for high-speed measurements. The implementation of a photonics system can drastically extend the measurable frequency of conventional electrical measurement systems at around 110 GHz. In addition, it can eliminate the troublesome process of combining the divided frequency band. We have realized a photonic network analyzer [65]–[68] probe for the time-domain measurements in a pump-and-probe scheme. A UTC-PD generates short electrical pulses when excited by subpicosecond optical pulses. Then, the electrical pulses propagate to the device-under-test on a 50-Ω CPW fabricated on quartz, which is designed to carry over 300-GHz bandwidth signals with small dispersion and

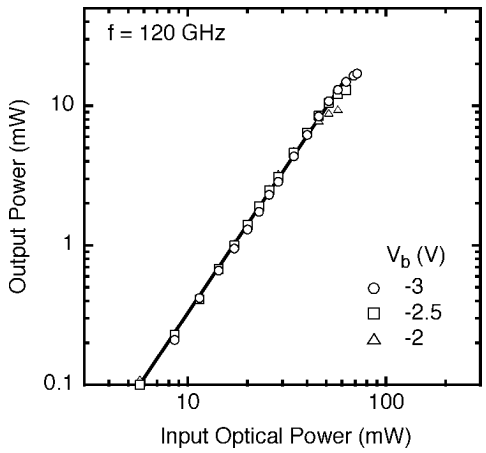

Fig. 23. Relationship between measured millimeter-wave output power and the diode photocurrent at 120 GHz.

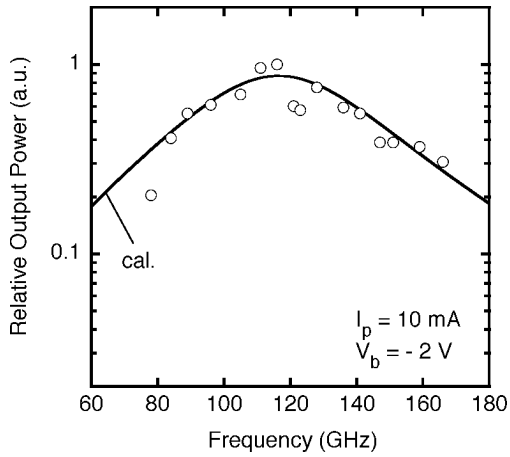

Fig. 24. Output powers from the module against frequency. Solid curve in the figure is a calculation based on an analytical model.

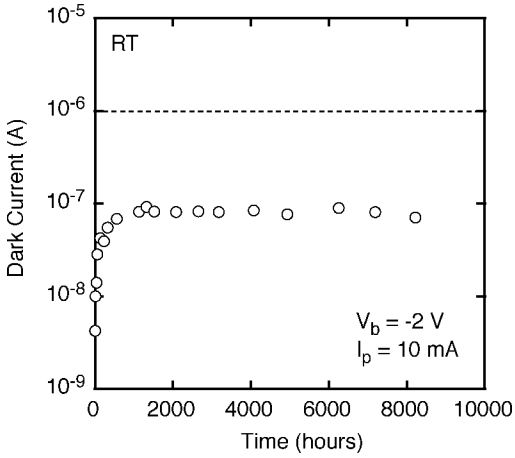

Fig. 25. Variation of the dark current of the W-band module against time under optical input and reverse bias stresses.

attenuation. The propagating electrical signals are measured in the time domain using the electrooptic sampling technique [29]. As an example, the frequency-domain S-parameters of a high electron mobility transistor (HEMT) with a 0.1-μm gate were measured and they agreed well with the results obtained by a conventional network analyzer. The total useful bandwidth (30-dB) is over 300 GHz.

One of the largest scale measurement systems is the radio telescope, which simultaneously requires extreme performance from all devices incorporated. There is an international project to build a large millimeter and submillimeter interferometer array (ALMA) consisting of 80 parabola antennas distributed within an area of $\sim$10 km^2 in northern Chile [69], [84]. This radio telescope will detect signals from the universe at frequencies from 30 to 950 GHz using superconductor–insulator–superconductor (SIS) mixers [85]. Simultaneously delivering a local signal to the multiple mixers within a maximum distance of 25 km while maintaining the signal phase for the interferometry can best be accomplished with a photonic system [69], [84]. This is because a photonic system provides an extremely wide bandwidth and can use low-loss fibers for transmission of very high-frequency signals. The proposed frequency configuration for the direct photonic local oscillator (LO) driver (in combination with amplifiers and multipliers) [86] requires photodiode modules that operate mostly in the 80–120-GHz band and some in the 100–160-GHz band. For practical use, especially in the frequency range above 100 GHz, the device should be in a module with a rectangular waveguide (WG) output port, because the useful frequency range of the coaxial connector is limited to below $\sim$100 GHz. We have developed a waveguide output UTC-PD module for operation in the F-band (90–140 GHz) [75].

Fig. 22 is a photograph of the fabricated butterfly-type module connected to the WR-8 rectangular waveguide for the F-band. Its size and configuration are equivalent to those of conventional semiconductor O/E devices so that it is compatible with the standard assembly/testing equipment for O/E device modules. The responsivity of the module is about 0.35 A/W.

Fig. 23 shows the relationship between the measured millimeter-wave output power and the diode photocurrent for the fabricated module at 120 GHz. Here, pulse trains from an actively mode-locked semiconductor laser diode operating at 60 GHz ($\lambda = 1.55$ μm) were optically multiplexed by using an optical multiplexer (OMUX) to prepare quasisinusoidal 120-GHz millimeter-wave optical input signal [87]. The output power was detected with a power meter. A wide linearity is maintained up to a very high millimeter-wave output power of over 10 mW. The saturation point of the output power increased with increasing bias voltage, and the maximum output power of 17 mW (at a photocurrent of 25 mA) with a very wide linearity range was obtained at a bias voltage of -3 V. To our knowledge, this is the highest millimeter-wave output power directly generated from a PD module in the F-band.

The output 3-dB bandwidth (Fig. 24) was about 55 GHz, which fully covers the F-band. The solid curve in the figure is a fitting calculation based on an analytical model of the matching circuit. The experimental result agrees well with the calculation, indicating that most of the frequency variation is that of the integrated matching circuit.

We have also developed a waveguide-output UTC-PD module for operation in the W-band (75–110 GHz) [76] and D-band (110–170 GHz) to fulfill the requirement for ALMA [85]. For practical use, long-term stability is also an important

issue. Although bias-temperature and optical-input stress tests have confirmed that UTC-PDs designed for 40 Gb/s optical communications systems have excellent reliability [44], we also measured the variation of dark current in the fabricated waveguide-output module under optical input stresses at room temperature (Fig. 25). Here, the W-band module [76] was used for the experiment. The module was biased at -2 V with an optical input corresponding to a photocurrent of 10 mA (responsivity is about 0.35 A/W). Except for an initial increase, the dark current stayed at a very low level for more than 8000 h. These values are considerably lower than the generally required level for high-speed PDs of 1 μA (broken line in Fig. 25). This indicates that the fabricated UTC-PD chip is reasonably reliable. The changes in responsivity and millimeter-wave output power at the same photocurrent were also confirmed to be very small after this long-term stability test.

A photonic LO [88] comprising a waveguide-output UTC-PD module [89] and a millimeter-wave light signal source based on an optical comb generator [90] has already been applied to radioastronomical observation [91]. By photonically supplying a local signal to the receiver in the 45-m telescope at Nobeyama Radio Observatory, Japan, we were able to successfully obtain spectra of CS molecules from W51 (H_2O) (a famous high-mass star-forming region in our galaxy) with a signal-to-noise ratio comparable with that of conventional electrical local signal source. This clearly indicates that the photonic local signal distribution system is practically applicable for radio telescopes.

In the frequency range above the D-band, monolithic integration of a photodiode and a miniaturized antenna [92] is promising because it eliminates the loss and reflection in electrical transmission lines. It may also be necessary to employ a quasi-optical system to configure a system that can handle submillimeter-wave signals. Fig. 26 shows a micrograph of the fabricated device, which integrates a UTC-PD and a self-complementary log-periodic toothed planar antenna, whose teeth correspond to frequencies from 150 GHz to 2.4 THz [23], [93]. Fig. 27 shows the relationship between the measured millimeter-wave output power and the diode photocurrent at 1.04 THz for a bias voltage of -2 V [94]. Here, the millimeter-wave power was measured using a Fourier transform spectrometer and an InSb hot-electron bolometer, and the absolute values were calibrated against a blackbody. The output power increased linearly in proportion to the square of the photocurrent, and the maximum output power obtained was 2.6 μW at a photocurrent of 13 mA. To our knowledge, this is the highest output power ever directly generated from a PD in the THz range. It is even higher than the highest output power reported for a low-temperature-grown (LT) GaAs photoconductive switch [95] and is more than two orders of magnitude higher than that obtained by a pin PD [96].

Here, the observed result includes power losses due to coupling efficiency, absorption, reflection, and divergence of the output signal, and emission toward the opposite side from the Si lens. Thus, the actual emitted power should be even higher. More importantly, the bias voltage applied was about an order smaller than that required for the LT-GaAs photoconductive switch [95]. Thus, the total power dissipation in the device is much smaller, which should be advantageous in regard to device

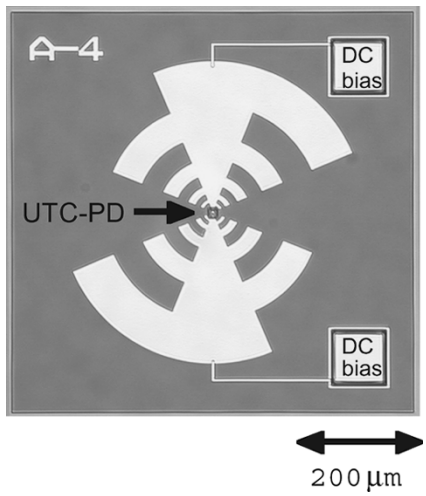

Fig. 26. Micrograph of a UTC-PD integrated with a log-periodic antenna.

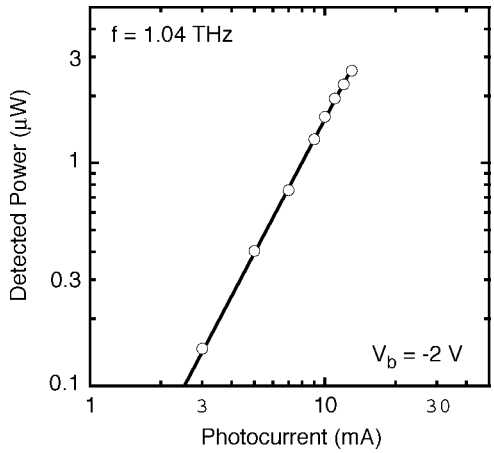

Fig. 27. Relationship between $P_{\rm out}$ and diode photocurrent at 1.04 THz.

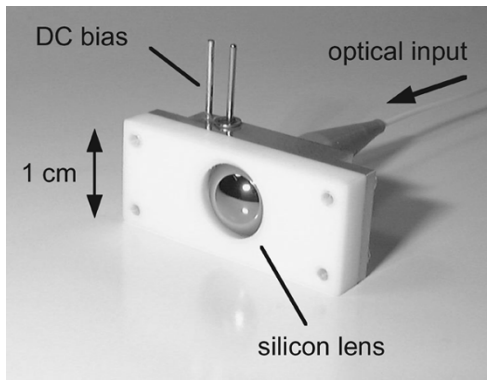

Fig. 28. Photograph of the quasioptic UTC-PD module with an Si lens.

reliability. We also obtained a record output power of 300 μW at 300 GHz from the same device [97].

For practical use, we have also fabricated a quasi-optical UTC-PD module (Fig. 28). We designed the module to be the same size as that of conventional semiconductor optoelectronic (O/E) devices so that we could use standard assembly equipment. The PD chip was placed on a hyper-hemispherical silicon lens and electrically connected to the dc bias leads. Then, the photodiode was optically coupled to the optical fiber using a

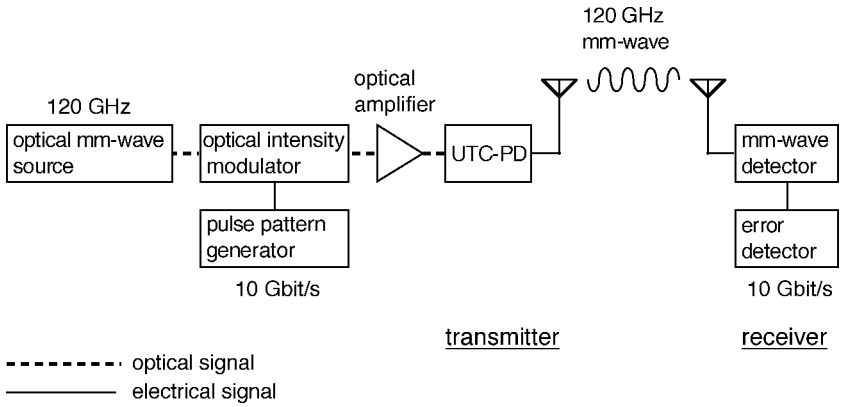

Fig. 30. Experimental setup for the 120-GHz wireless link using a UTC-PD in the photonic millimeter-wave emitter.

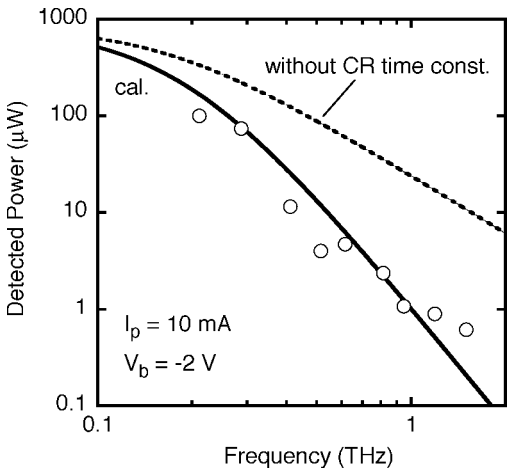

Fig. 29. Frequency dependence of the detected power from the quasioptic module. Solid curve is the calculation based on the device parameters, and the broken curve is the one without the CR time constant.

single-lens system. These optical parts were welded onto the package using a YAG laser, which assures the stability of the optical alignment. The size of the module is $12.7\times30\times10$ mm (excluding the optical fiber and the leads).

Fig. 29 shows the frequency characteristics of the fabricated module for a photocurrent of 10 mA. The output power decreased gradually with increasing frequency, and we could detect submillimeter waves at frequencies of up to 1.5 THz. This is the highest operation frequency ever achieved using a photodiode operating at 1.55 μm. The solid curve in the figure is a calculation, which only takes into account the CR-limited and transit-time limited bandwidths [23] of the UTC-PD with a constant loss. The experimental result agrees well with the calculation, indicating that only the PD device parameters are determining the basic frequency dependence and that the integrated antenna is very wideband. Thus, if we can eliminate the influence of the CR time constant by employing a resonating narrow-band matching circuit, it would be possible to obtain an output power of more than 10 μW at 1 THz, as indicated by the broken curve in the figure. These results clearly indicate that the UTC-PD is a promising and realistic device for generating a continuous THz wave with a practical output power, which is required in various applications, such as submillimeter-wave spectroscopy, imaging, and probes for investigating the influences of electromagnetic waves on biological objects.

Photonic generation of millimeter-/submillimeter-wave signal is also promising for the millimeter-wave imaging systems [19], [67], [68]. This technology allows us to obtain information through optically nontransparent obstacles, such as thin walls, fog, or smoke. The prospective application areas include security systems, millimeter-wave scopes for emergency situations, inspection of agricultural and industrial products, and medical diagnosis.

C. Transmitter for Fiber-Radio Communications Systems

Another promising analog application of the high-output UTC-PD is fiber-radio wireless communications systems. The growing demand for expanding data throughput in wireless communications system has been accelerating the use of frequencies up to the millimeter-wave range. As the frequency becomes higher, the electrical transmission of the microwave/millimeter-wave signal from the central station to the base station becomes more difficult due to the large loss in a coaxial cable. One approach to overcoming this problem is to use photonics technology. In addition, the use of a high-output-power PD can eliminate the costly post amplification circuit and simplify the base station.

Fig. 30 shows the experimental setup for a 120-GHz wireless link using a UTC-PD in the photonic millimeter-wave emitter [98]. For the optical millimeter-wave signal source, pulse trains from a subharmonically mode-locked laser diode operating at 60 GHz were optically multiplexed by using an OMUX to prepare quasisinusoidal 120-GHz millimeter-wave light signal $(\lambda = 1.55\ \mu\text{m})$ [87]. The 120-GHz optical carrier was coded by a Mach–Zehnder modulator (MZM) using PRBS signals generated from a pulse pattern generator (PPG). A modulated subcarrier was fed into the photonic emitter and was converted into millimeter-wave signals. The photonic emitter consists of a UTC-PD, a HEMT amplifier, and a waveguide-coupled antenna and can output millimeter-wave output power of up to 7.3 mW at 120 GHz. The millimeter-wave signal was transmitted over a distance of 2.5 m and detected by a Schottky barrier diode detector.

Fig. 31 shows the dependence of the BER on the received millimeter-wave power. A BER of less than 10^{-10} was obtained

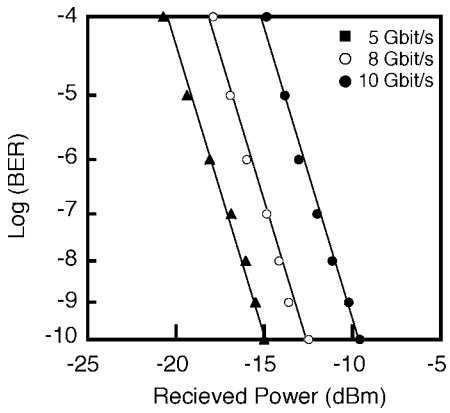

Fig. 31. BER performance of the 120-GHz-band wireless link.

when the received power was −9.6 dBm at 10 Gb/s, −12.5 dBm at 8 Gb/s, and −15.0 dBm at 5 Gb/s. The transmission rate of 10 Gb/s [98]–[100] is the highest ever achieved in a millimeter-wave wireless link and is about an order of magnitude higher than that obtained by a pure electronics-based system (1.25 Gb/s at 60 GHz) [101].

We have also developed a compact photonic emitter module for a 60-GHz wireless link [102] using a device monolithically integrating a UTC-PD, a planar antenna, and a bias circuit [103]. With this module, error-free transmission at a bit rate of up to 2.5 Gb/s has been demonstrated [102]. These results are highly promising for realizing broadband wireless communications systems that overcome the limitations of today's electronics-based ones.

D. Nonlinear Photonic Up-Conversion

Another application is photonic millimeter-wave frequency conversion based on nonlinear operation of a UTC-PD. In order to simplify the configuration of frequency conversion and suppress the chromatic dispersion effect, direct frequency conversion using nonlinear photodiode operation is promising [104]. For realizing such a function, stronger nonlinearity as well as possible high output level of converted millimeter-wave signal is important. A conventional pin PD has output nonlinearity in its response. The nonlinearity originates from carrier velocity modulation, which depends on diode operation voltage and carrier space charges. However, the conversion efficiency is relatively low compared with that of more conventional methods based on electrical mixing using varactors or field effect transistors. As we have seen (Figs. 3, 20, 23, and 27), the UTC-PD has a high linearity up to a very high output range. The important point here is that, when the output saturation occurs in the UTC-PD, the output deviates from the linear tendency rapidly; that is, there is a strong nonlinearity. By effectively using this characteristic, we can realize an efficient and high-output-power frequency converter.

We have demonstrated photonic frequency up-conversion (photomixing) in the millimeter-wave range [105] using the setup shown in Fig. 32. The UTC-PD was biased at 0 V, where the nonlinearity becomes much stronger. Two RF modulated lights, one fixed at a local frequency (59.4 GHz) and the other variable in the intermediate frequency range (600 MHz), were

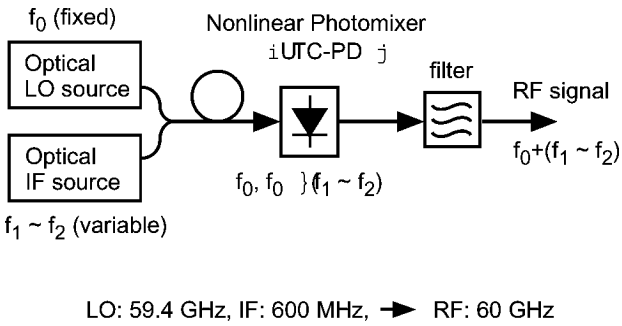

Fig. 32. Experimental setup for the nonlinear frequency up-conversion using a UTC-PD.

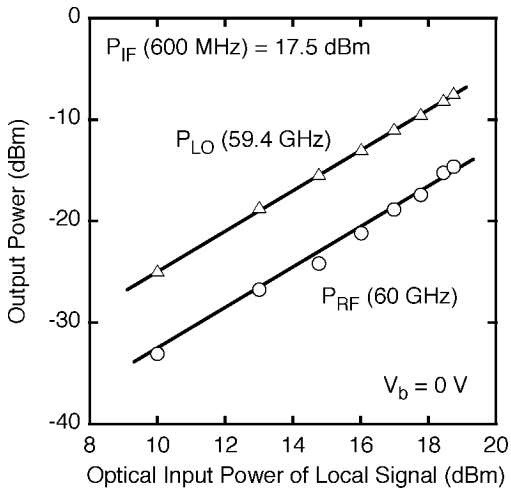

Fig. 33. Output LO power and up-converted signal power against the input power of optical local signal. IF input power was kept constant at 17.5 dBm.

optically mixed and fed into a UTC-PD through an optical fiber, and the millimeter-wave output power was measured by a spectrum analyzer. Fig. 33 shows the variations of millimeter-wave power for local and up-converted signals against the optical local input power. Here, the optical power for the intermediate frequency signal was kept constant at 17.5 dBm. The up-converted signal power at 60 GHz increases almost linearly with the square of optical input power. The conversion efficiency was as high as −8 dB for the measured range. This conversion efficiency is the highest ever reported for photonic millimeter-wave frequency conversion using a photodiode and more than an order of magnitude larger than that reported for a pin PD [104]. Moreover, the output power improvement is more than 30 dB, which clearly demonstrates practical output power for various applications. Since the modulation of optical signals at frequencies of several gigahertz can be easily accomplished by means of today's low-cost optical components, this configuration enables us to generate very high frequency signals with a wide variable frequency range of up to several gigahertz in a cost-effective way.

VII. Conclusion

The basics of the UTC-PD, such as its operations, fabrication, bandwidth, output level, low-bias-voltage operation, efficiency, and reliability, were overviewed. The UTC-PD

has a unique mode of operation and is capable of high-speed and high-output operations. UTC-PDs exhibit a record 3-dB bandwidth of over 300 GHz and a record RF output power of over 20 mW at 100 GHz. As promising digital applications, a UTC-PD photoreceiver at bit rates of up to 160 Gb/s and error-free DEMUX operation of a novel PD-EAM optical gate (integrating a UTC-PD and a TW-EAM) at bit rates of up to 320 Gb/s have been demonstrated. Integration of the UTC-PD with various electronic devices is also promising. As analog applications, we have developed a waveguide output UTC-PD module and demonstrated an output power of 17 mW at 120 GHz. A quasi-optic UTC-PD module also exhibits a record output power of 2.6 μW at 1.04 THz. With this excellent performance, these modules are suitable for several analog applications, such as fiber-radio wireless communication systems at a data rate of up to 10 Gb/s, millimeter-wave imaging systems, RF sources for measurement equipment, photonic frequency conversion, and the local signal distribution system in radio telescopes.

ACKNOWLEDGMENT

The authors would like to thank the technical members of NTT Laboratories, especially A. Hirata, Y. Hirota, K. Yoshino, H. Fushimi, T. Ohno, T. Ito, T. Yoshimatsu, and F. Nakajima for their valuable discussions, and J. Yumoto for his continuous encouragement. They also thank Prof. M. Ishiguro of the National Astronomical Observatory of Japan for his stimulating discussions on photonic millimeter-wave sources.

REFERENCES

[1] K. Fukuchi, T. Kasamatsu, M. Morie, R. Ohhira, T. Ito, K. Sekiya, D. Ogasahara, and T. Ono, "10.92-Tb/s (273 × 40-Gb/s) triple-band/ultra-dense WDM optical-repeatered transmission experiment," in *Tech. Dig. Optical Fiber Communication Conf.*, 2001, PD24.

[2] A. J. Seeds, "Broadband wireless access using millimeter-wave over fiber systems," in *Tech. Dig. Int. Microwave Symp.*, 1997, pp. 23–25.

[3] T. Nagatsuma, "Progress in instrumentation and measurement toward millimeter-wave photonics," in *Tech. Dig. Int. Topical Meeting Microwave Photonics*, 1999, pp. 91–94.

[4] K. Kato, S. Hata, K. Kawano, and A. Kozen, "Design of ultrawide-band, high-sensitivity p-i-n photodetectors," *IEICE Trans. Electron.*, vol. E76-C, pp. 214–221, 1993.

[5] K. Hagimoto, Y. Miyamoto, T. Kataoka, H. Ichino, and O. Nakajima, "Twenty-Gb/s signal transmission using simple high-sensitivity optical receiver," in *Tech. Dig. 16th Optical Fiber Communication Conf.*, 1992, p. 48.

[6] Y. Miyamoto, M. Yoneyama, T. Otsuji, K. Yonenaga, and N. Shimizu, "40-Gbits/s TDM transmission technologies based on ultra-high-speed ICs," *IEEE J. Solid-State Circuits*, vol. 34, pp. 1246–1253, Sept. 1999.

[7] T. Furuta, H. Ito, and T. Ishibashi, "Photocurrent dynamics of uni-traveling-carrier and conventional pin-photodiodes," *Proc. Inst. Phys. Conf. Ser.*, no. 166, pp. 419–422, 2000.

[8] T. Ishibashi, N. Shimizu, S. Kodama, H. Ito, T. Nagatsuma, and T. Furuta, "Uni-traveling-carrier photodiodes," in *Tech. Dig. Ultrafast Electronics Optoelectronics OSA Spring Topical Meeting*, 1997, pp. 166–168.

[9] T. Ishibashi, T. Furuta, H. Fushimi, S. Kodama, H. Ito, T. Nagatsuma, N. Shimizu, and Y. Miyamoto, "InP/InGaAs uni-traveling-carrier photodiodes," *IEICE Trans. Electron.*, vol. E83-C, pp. 938–949, 2000.

[10] T. Ishibashi, S. Kodama, N. Shimizu, and T. Furuta, "High-speed response of uni-traveling carrier photodiodes," *Jpn. J. Appl. Phys.*, vol. 36, pp. 6263–6268, 1997.

[11] T. Ishibashi, T. Furuta, H. Fushimi, and H. Ito, "Photoresponse characteristics of uni-traveling-carrier photodiodes," *Proc. SPIE*, vol. 4283, pp. 469–479, 2001.

[12] H. Ito, T. Furuta, S. Kodama, and T. Ishibashi, "InP/InGaAs uni-travelling-carrier photodiode with a 310 GHz bandwidth," *Electron. Lett.*, vol. 36, pp. 1809–1810, Oct. 2000.

[13] H. Ito, T. Nagatsuma, A. Hirata, T. Minotani, A. Sasaki, Y. Hirota, and T. Ishibashi, "High-power photonic millimeter-wave generation at 100 GHz using matching-circuit-integrated uni-travelling-carrier photodiodes," *Proc. Inst. Elect. Eng. Optoelectron.*, vol. 150, pp. 138–142, 2003.

[14] Y. Miyamoto, K. Yonenaga, A. Hirano, N. Shimizu, M. Yoneyama, H. Takara, K. Noguchi, and K. Suzuki, "1.04-Tbit/s DWDM transmission experiment based on alternate-polarization 80-Gb/s OTDM signals," in *Proc. 24th Eur. Conf. Optical Communication*, vol. 3, 1998, pp. 55–57.

[15] M. Yoneyama, Y. Miyamoto, T. Otsuji, H. Toba, Y. Yamane, T. Ishibashi, and H. Miyazawa, "Fully electrical 40-Gb/s TDM system prototype based on InP HEMT digital IC technologies," *J. Lightwave Technol.*, vol. 18, pp. 34–43, 2000.

[16] T. Ohno, S. Fukushima, Y. Doi, Y. Muramoto, and Y. Matsuoka, "Application of uni-traveling-carrier waveguide photodiodes in base stations of a millimeter-wave fiber-radio system," in *Tech. Dig. Int. Topical Meeting Microwave Photonics*, 1999, pp. 253–256.

[17] A. Hirata, H. Ishii, and T. Nagatsuma, "Design and characterization of a 120-GHz millimeter-wave antenna for integrated photonic transmitters," *IEEE Trans. Microwave Theory Tech.*, vol. 49, pp. 2157–2162, Nov. 2001.

[18] N. Sahri and T. Nagatsuma, "Packaged photonic probes for an on-wafer broad-band millimeter-wave network analyzer," *IEEE Photon. Technol. Lett.*, vol. 12, pp. 1225–1227, Sept. 2000.

[19] A. Sasaki and T. Nagatsuma, "Reflection-type CW-millimeter-wave imaging with a high-sensitivity waveguide-mounted electro-optic sensor," *Jpn. J. Appl. Phys.*, vol. 41, pp. L83–L86, 2002.

[20] N. Shimizu, K. Murata, A. Hirano, Y. Miyamoto, H. Kitabayashi, Y. Umeda, T. Akeyoshi, T. Furuta, and N. Watanabe, "40 Gb/s monolithic digital OEIC composed of unitraveling-carrier photodiode and InP HEMTs," *Electron. Lett.*, vol. 36, pp. 1220–1222, July 2000.

[21] S. Kodama, T. Ito, N. Watanabe, S. Kondo, H. Takeuchi, H. Ito, and T. Ishibashi, "2.3 picoseconds optical gate monolithically integrating photodiode and electroabsorption modulator (PD-EAM)," *Electron. Lett.*, vol. 37, pp. 1185–1186, Sept. 2001.

[22] H. Ito, Y. Hirota, A. Hirata, T. Nagatsuma, and T. Ishibashi, "11 dBm photonic millimeter-wave generation at 100 GHz using uni-travelling-carrier photodiode," *Electron. Lett.*, vol. 37, pp. 1225–1226, 2001.

[23] H. Ito, T. Furuta, Y. Hirota, T. Ishibashi, A. Hirata, T. Nagatsuma, H. Matsuo, T. Noguchi, and M. Ishiguro, "Photonic millimeter-wave emission at 300 GHz using an antenna-integrated uni-traveling-carrier photodiode," *Electron. Lett.*, vol. 38, pp. 989–990, 2002.

[24] A. Hirata, T. Nagatsuma, R. Yano, H. Ito, T. Furuta, Y. Hirota, T. Ishibashi, H. Matsuo, A. Ueda, T. Noguchi, Y. Sekimoto, M. Ishiguro, and S. Matsuura, "Output power measurement of photonic millimeter-wave and sub-millimeter-wave emitter at 100–800 GHz," *Electron. Lett.*, vol. 38, pp. 798–800, 2002.

[25] T. Ishibashi, "High speed heterostructure devices," in *Semiconductors and Semimetals*. San Diego, CA: Academic, 1994, vol. 41, ch. 5, p. 333.

[26] E. S. Harmon, M. L. Lovejoy, M. R. Melloch, M. S. Lundstrom, D. Ritter, and R. A. Hamm, "Minority-carrier mobility enhancement in p+ InGaAs lattice matched to InP," *Appl. Phys. Lett.*, vol. 63, pp. 636–638, 1993.

[27] H. Ito, T. Furuta, S. Kodama, and T. Ishibashi, "Zero-bias high-speed and high-output-voltage operation of cascade-twin uni-travelling-carrier photodiode," *Electron. Lett.*, vol. 36, pp. 2034–2036, Nov. 2000.

[28] N. Shimizu, N. Watanabe, T. Furuta, and T. Ishibashi, "Improved response of uni-traveling-carrier photodiodes by carrier injection," *Jpn. J. Appl. Phys.*, pt. 1, vol. 37, pp. 1424–1426, 1997.

[29] T. Nagatsuma, M. Yaita, M. Shinagawa, K. Kato, A. Kozen, K. Iwatsuki, and K. Suzuki, "Electro-optic characterization of ultrafast photodetectors using adiabatically compressed soliton pulses," *Electron. Lett.*, vol. 30, pp. 814–816, 1994.

[30] T. H. Windhorn, L. W. Cook, M. A. Haase, and G. E. Stillman, "Electron transport in InP at high electric fields," *Appl. Phys. Lett.*, vol. 42, pp. 725–727, 1983.

[31] H. Ito, T. Furuta, and T. Ishibashi, "InP/InGaAs uni-traveling-carrier photodiodes," *IEICE Trans. Electron.*, vol. E83-C, pp. 938–949, 2000.

[32] P. Hill, J. Schlafer, W. Powazinik, M. Urban, E. Eichen, and R. Olshansky, "Measurement of hole velocity in n-type InGaAs," *Appl. Phys. Lett.*, vol. 50, pp. 1260–1262, 1987.

[33] H. Ito, T. Furuta, S. Kodama, N. Watanabe, and T. Ishibashi, "InP/InGaAs uni-traveling-carrier photodiode with 220 GHz bandwidth," *Electron. Lett.*, vol. 35, pp. 1556–1557, 1999.

[34] O. Madelung, M. Schultz, and H. Weiss, "Numerical data in science and technology," in *Landolt-Boernstein*. Berlin, Germany: Springer-Verlag, 1982, vol. 17, p. 571.

[35] J. C. Aquino, T. Kawashima, and M. Tokuda, "Evaluation of anechoic chamber characteristics using optically driven equipment under test," in *Proc. IEEE Int. Symp. EMC*, 1999, pp. 231–233.

[36] K. Kato, A. Kozen, Y. Muramoto, Y. Itaya, T. Nagatsuma, and M. Yaita, "110-GHz, 50%-efficiency mushroom-mesa waveguide p-i-n photodiode for a 1.55-mm wavelength," *IEEE Photon. Technol. Lett.*, vol. 6, pp. 719–721, 1994.

[37] Y.-G. Wey, K. Giboney, J. Bowers, M. Rodwell, P. Silvestre, P. Thiagarajan, and G. Robinson, "110-GHz GaInAs/InP double heterostructure p-i-n photodetectors," *J. Lightwave Technol.*, vol. 13, pp. 1490–1499, July 1995.

[38] H. Ito, T. Ohno, H. Fushimi, T. Furuta, S. Kodama, and T. Ishibashi, "60 GHz high output power uni-travelling-carrier photodiodes with integrated bias circuit," *Electron. Lett.*, vol. 36, pp. 747–748, Apr. 2000.

[39] Y. Muramoto, K. Kato, M. Mitsuhara, O. Nakajima, Y. Matsuoka, N. Shimizu, and T. Ishibashi, "High-output voltage, high speed, high efficiency uni-traveling-carrier waveguide photodiode," *Electron. Lett.*, vol. 34, pp. 122–123, Jan. 1998.

[40] H. Fukano, Y. Muramoto, K. Takahata, and Y. Matsuoka, "High-efficiency edge-illuminated uni-traveling-carrier-structure refracting-facet photodiode," *Electron. Lett.*, vol. 35, pp. 1664–1665, 1999.

[41] H. Ito, T. Furuta, S. Kodama, and T. Ishibashi, "High-efficiency uni-traveling-carrier photodiode with an integrated total-reflection mirror," *J. Lightwave Technol.*, vol. 18, pp. 384–387, Mar. 2000.

[42] Y. Muramoto, H. Fukano, T. Furuta, and Y. Matsuoka, "A polarization-independent high-efficiency refracting-facet uni-traveling-carrier photodiode with a bandwidth over 50 GHz," in *Proc. 26th Eur. Conf. Optical Communication*, vol. 2, 2000, pp. 109–110.

[43] L. Y. Lin, M. C. Wu, T. Itoh, T. A. Vang, R. E. Muller, D. L. Sivco, and A. Y. Cho, "Velocity-matched distributed photodetectors with high-saturation power and large bandwidth," *IEEE Photon. Technol. Lett.*, vol. 8, pp. 1376–1378, Oct. 1996.

[44] Y. Hirota, T. Ishibashi, and H. Ito, "1.55-μm wavelength periodic traveling-wave photodetector fabricated using unitraveling-carrier photodiode structures," *J. Lightwave Technol.*, vol. 19, pp. 1751–1758, Nov. 2001.

[45] T. Furuta, H. Fushimi, T. Yasui, Y. Muramoto, H. Kamioka, H. Mawatari, H. Fukano, T. Ishibashi, and H. Ito, "Reliability study on uni-traveling-carrier photodiode for a 40 Gb/s optical transmission systems," *Electron. Lett.*, vol. 38, pp. 332–334, 2002.

[46] Y. Muramoto, Y. Hirota, K. Yoshino, H. Ito, and T. Ishibashi, "Uni-travelling-carrier photodiode module with a bandwidth of 80 GHz," *Electron. Lett.*, vol. 39, pp. 1851–1852, Dec. 2003.

[47] Y. Muramoto, K. Yoshino, S. Kodama, Y. Hirota, H. Ito, and T. Ishibashi, "100- and 160-Gb/s operations of uni-traveling-carrier photodiode module," *Electron. Lett.*, vol. 40, pp. 378–380, 2004.

[48] A. Beling, H.-G. Bach, G. G. Mekonnen, T. Eckhardt, R. Kunkel, G. Jacumeit, M. Kroh, and J. Berger, "Fully packaged InP-based photodetector for 80/85 Gb/s RZ systems," in *Proc. 29th Eur. Conf. Optical Communication*, vol. 6, 2003, pp. 82–83.

[49] A. Konczykowska, F. Jorge, A. Kasbari, W. Idler, L. Giraudet, K. Schuh, B. Junginger, and J. Godin, "High-sensitivity decision circuit in InP/InGaAs DHBT technology and 40–80 Gb/s optical experiments," *Electron. Lett.*, vol. 39, pp. 1532–1533, Oct. 2003.

[50] S. Kodama, T. Yoshimatsu, T. Ito, H. Ito, and T. Ishibashi, "160-Gb/s error-free demultiplexing by ultrafast optical gate monolithically integrating photodiode and electroabsorption modulator," *Electron. Lett.*, vol. 38, pp. 1575–1576, Nov. 2002.

[51] S. Kodama, T. Yoshimatsu, and H. Ito, "320-Gb/s error-free demulplexing by using an ultrafast optical gate monolithically integrating a photodiode and electroabsorption modulator," *Electron. Lett.*, vol. 39, pp. 1269–1270, 2003.

[52] ——, "500-Gb/s demultiplexing operation of a monolithic PD-EAM optical gate," in *Tech. Dig. 29th Eur. Conf. Optical Communication*, vol. 6, 2003, pp. 58–59.

[53] T. Yoshimatsu, S. Kodama, K. Yoshino, and H. Ito, "100-Gb/s full-rate operation of PD-EAM optical gate for retiming function," in *Extended Abst. Int. Conf. Solid State Devices and Materials*, 2003, pp. 882–883.

[54] S. Kodama, T. Shimizu, T. Yoshimatsu, K. Yoshino, T. Furuta, and H. Ito, "Ultrafast optical sampling gate monolithically integrating a photodiode and an electroabsorption modulator," *Electron. Lett.*, vol. 40, pp. 696–697, May 2004.

[55] M. Yoneyama, Y. Miyamoto, N. Shimizu, K. Hagimoto, and T. Ishibashi, "Simple wavelength converter using an optical modulator directly driven by a uni-travelling-carrier photodiode," *Electron. Lett.*, vol. 34, pp. 2244–2245, Nov. 1998.

[56] H. Kitabayashi, Y. Umeda, T. Furuta, N. Watanabe, T. Akeyoshi, Y. Yamane, K. Murata, N. Shimizu, and Y. Ishii, "Monolithic integration technology using InP-based HEMT's and a uni-traveling-carrier-photodiode for over 40 Gb/s digital OEIC," in *Proc. Int. Conf. Indium Phosphide Related Materials*, 2000, pp. 329–332.

[57] K. Murata, H. Kitabayashi, N. Shimizu, S. Kimura, T. Furuta, N. Watanabe, and E. Sano, "A 40-Gb/s monolithic digital OEIC module composed of uni-traveling-carrier photodiode and InP HEMT decision circuit," in *Proc. 2000 IEEE MTT-S Int. Microwave Symp. Dig.*, 2000, pp. 345–248.

[58] K. Sano, K. Murata, H. Matsuzaki, H. Kitabayashi, T. Akeyoshi, H. Ito, T. Enoki, and H. Sugahara, "75-GHz optical clock device-by-two OEIC using InP HEMT and uni-traveling-carrier photodiode," in *Proc. Extended Abstract Int. Conf. Solid State Devices and Materials*, 2003, pp. 902–903.

[59] K. Sano, K. Murata, T. Akeyoshi, N. Shimizu, T. Otsuji, M. Yamamoto, T. Ishibashi, and E. Sano, "An ultra-fast optoelectronic circuit using resonant tunneling diodes and a uni-traveling-carrier photodiode," *Electron. Lett.*, vol. 34, pp. 215–217, 1998.

[60] T. Akeyoshi, N. Shimizu, J. Osaka, M. Yamamoto, T. Ishibashi, K. Sano, K. Murata, and E. Sano, "An optoelectronic logic gate monolithically integrating resonant tunneling diodes and a uni-traveling-carrier photodiode," *Jpn. J. Appl. Phys.*, vol. 38, pp. 1223–1226, 1999.

[61] K. Sano, K. Murata, T. Otsuji, T. Akeyoshi, N. Shimizu, and E. Sano, "80 Gb/s optoelectronic delayed flip-flop circuit using resonant tunneling diodes and uni-traveling-carrier photodiode," *Electron. Lett.*, vol. 35, pp. 1376–1377, Aug. 1999.

[62] K. Sano, K. Murata, T. Otsiji, T. Akeyoshi, N. Shimizu, M. Yamamoto, T. Ishibashi, and E. Sano, "Ultra-fast optoelectronic decision circuit using resonant tunneling diodes and a uni-traveling-carrier photodiode," *IEICE Trans. Electron.*, vol. E82-C, pp. 1638–1646, 1999.

[63] K. Murata, K. Sano, T. Akeyoshi, N. Shimizu, E. Sano, M. Yamamoto, and T. Ishibashi, "Optoelectronic clock recovery circuit using a resonant tunneling diode and uni-travelling-carrier photodiode," *Electron. Lett.*, vol. 34, pp. 1424–1425, July 1998.

[64] ——, "An optoelectronic clock recovery circuit using a resonant tunneling diode and a uni-traveling-carrier photodiode," *IEICE Trans. Commun.*, vol. E-82-B, pp. 1228–1235, 1999.

[65] T. Otsuji, N. Sahri, N. Shimizu, T. Nagatsuma, and T. Ishibashi, "A 105-GHz bandwidth optical-to-electrical conversion stimulus probe head employing a unitraveling-carrier photodiode," *IEEE Photonics Technol. Lett.*, vol. 11, pp. 1033–1035, Aug. 1999.

[66] N. Sahri and T. Nagatsuma, "Application of 1.55-μm photonic technology to practical millimeter-wave network analysis," *IEICE Trans. Electron.*, vol. E82-C, pp. 1307–1311, 1999.

[67] A. Sasaki and T. Nagatsuma, "Millimeter-wave imaging using an electrooptic detector as a harmonic mixer," *IEEE J. Selected Topics Quantum Electron.*, vol. 6, pp. 735–740, Sept./Oct. 2000.

[68] T. Nagatsuma, "Photonic measurement technologies for high-speed electronics," *Meas. Sci. Technol.*, vol. 13, pp. 1655–1663, 2002.

[69] J. Payne, B. Shillue, and A. Vaccari, "Photonic techniques for use on the Atacama large millimeter array," in *Tech. Dig. Int. Topical Meeting Microwave Photonics*, 1999, pp. 105–108.

[70] T. Nagatsuma, T. Ishibashi, A. Hirata, Y. Hirota, T. Minotani, A. Sasaki, and H. Ito, "Characterization of uni-travelling-carrier photodiode monolithically integrated with matching circuit," *Electron. Lett.*, vol. 37, pp. 1246–1247, 2001.

[71] P. G. Huggard, B. N. Ellison, P. Shen, N. J. Gomes, P. A. Davis, W. P. Shillue, A. Vaccari, and J. M. Payne, "Generation of millimeter and submillimeter waves by photomixing in 1.55 μm wavelength photodiode," *Electron. Lett.*, vol. 38, pp. 327–328, 2002.

[72] T. Nagatsuma, N. Sahri, M. Yaita, T. Ishibashi, N. Shimizu, and K. Sato, "All optoelectronic generation and detection of millimeter-wave signals," in *Tech. Dig. Int. Topical Meeting Microwave Photonics*, 1998, pp. 5–8.

[73] N. Shimizu, Y. Miyamoto, A. Hirano, K. Sato, and T. Ishibashi, "RF saturation mechanism of InP/InGaAs uni-travelling-carrier photodiode," *Electron. Lett.*, vol. 36, pp. 750–751, Apr. 2000.

[74] H. Ito, H. Fushimi, Y. Muramoto, T. Furuta, and T. Ishibashi, "High-power photonic microwave generation at K- and Ka-bands using a uni-traveling-carrier photodiode," *J. Lightwave Technol.*, vol. 20, pp. 1500–1505, Aug. 2002.

[75] H. Ito, T. Ito, Y. Muramoto, T. Furuta, and T. Ishibashi, "Rectangular waveguide output uni-traveling-carrier photodiode module for high-power photonic millimeter-wave generation in the F-band," *J. Lightwave Technol.*, vol. 21, pp. 3456–3462, Dec. 2003.

[76] H. Ito, T. Furuta, T. Ito, Y. Muramoto, K. Tsuzuki, K. Yoshino, and T. Ishibashi, "W-band uni-travelling-carrier photodiode module for high-power photonic millimeter-wave generation," *Electron. Lett.*, vol. 38, pp. 1376–1377, Oct. 2002.

[77] N. Li, X. Li, S. Demiguel, X. Zheng, J. C. Campbell, D. A. Tulchinsky, K. Williams, T. D. Isshiki, G. S. Kinsey, and R. Sudharsansan, "High-saturation-current charge-compensated InGaAs/InP uni-traveling-carrier photodiode," in *Proc. IEEE LEOS Annu. Meeting*, 2003, pp. 790–791.

[78] K. J. Williams, R. D. Esman, and M. Dagenais, "Nonlinearities in p-i-n microwave photodetectors," *J. Lightwave Technol.*, vol. 14, pp. 84–96, Jan. 1996.

[79] G. Unterbörsch, D. Trommer, A. Umbach, and G. G. Mekonnen, "High-bandwidth 1.55 μm waveguide integrated photodetector," in *Proc. 8th Int. Conf. Indium Phosphide Related Materials*, 1996, pp. 203–206.

[80] P. G. Huggard, B. N. Ellison, P. Shen, N. J. Gomes, P. A. Davis, W. P. Shillue, A. Vaccari, and J. M. Payne, "Efficient generation of guided millimeter-wave power by photomixing," *IEEE Photon. Technol. Lett.*, vol. 14, pp. 197–199, Feb. 2002.

[81] A. Hirata, M. Harada, and T. Nagatsuma, "120-GHz wireless link using photonic techniques for generation, modulation, and emission of millimeter-wave signals," *J. Lightwave Technol.*, vol. 21, pp. 2145–2153, Oct. 2003.

[82] T. Ohno, K. Sato, R. Iga, Y. Kondo, T. Furuta, K. Yoshino, and H. Ito, "A 160-GHz actively mode-locked semiconductor laser," *Electron. Lett.*, vol. 39, pp. 520–521, 2003.

[83] J. T. Ong, R. Takahashi, M. Tsuchiya, S.-H. Wong, R. T. Sahara, Y. Ogawa, and T. Kamiya, "Subpicosecond soliton compression of gain switched diode laser pulses using an Erbium-doped fiber amplifier," *IEEE J. Quantum Electron.*, vol. 29, pp. 1701–1707, June 1993.

[84] ALMA (Atacama Large Millimeter Array) Project *http://www.alma.nrao.edu/, http://www.eso.org/projects/alma/, http://www.nro.nao.ac.jp/~lmsa/index-j.html* [Online]

[85] ALMA Project Book *http://www.alma.nrao.edu/projectbk/construction/* [Online]

[86] ALMA Memo #435 (2002). *http://www.cv.nrao.edu/alma/almaweb/www/memos/* [Online]

[87] A. Hirata, M. Harada, and T. Nagatsuma, "3-Gb/s wireless data transmission using a millimeter-wave photonic techniques," in *Tech. Dig. 3rd Japan-Korea Joint Workshop Microwave Millimeter-Wave Photonics*, 2002, pp. 95–98.

[88] A. Ueda, T. Noguchi, S. Asayama, H. Iwashita, Y. Sekimoto, M. Ishiguro, H. Ito, T. Nagatsuma, A. Hirata, and W. Shillue, "Ultra-low noise photonic local oscillator at 100 GHz," *Jpn. J. Appl. Phys.*, vol. 42, pp. L704–L705, 2003.

[89] A. Ueda, T. Noguchi, H. Iwashita, Y. Sekimoto, M. Ishiguro, S. Takano, T. Nagatsuma, H. Ito, A. Hirata, and T. Ishibashi, "W-band waveguide photomixer using a uni-traveling-carrier photodiode with 2 mW output," *IEEE Trans. Microwave Theory Tech.*, vol. 51, pp. 1455–1459, May 2003.

[90] T. Yamamoto, H. Takara, and S. Kawanishi, "Generation and transmission of tunable terahertz optical clock," in *Tech. Dig. Int. Topical Meeting Microwave Photonics*, 2002, pp. 97–100.

[91] S. Takano, A. Ueda, T. Yamamoto, S. Asayama, Y. Sekimoto, T. Noguchi, M. Ishiguro, H. Takara, S. Kawanishi, H. Ito, A. Hirata, and T. Nagatsuma, "The first observation with photonic local oscillator," *Astronom. Soc. Japan*, vol. 55, pp. L53–L56, 2003.

[92] A. Stöhr, R. Heinzelmann, K. Hagedorn, R. Güsten, F. Schäfer, H. Stüer, F. Siebe, P. van der Wal, V. Krozer, M. Feiginov, and D. Jäger, "Integrated 460 GHz photonic transmitter module," *Electron. Lett.*, vol. 37, pp. 1347–1348, Oct. 2001.

[93] A. Hirata, T. Nagatsuma, R. Yano, H. Ito, T. Furuta, Y. Hirota, T. Ishibashi, H. Matsuo, A. Ueda, T. Noguchi, Y. Sekimoto, M. Ishiguro, and S. Matsuura, "Output power measurement of photonic millimeter-wave and sub-millimeter-wave emitter at 100–800 GHz," *Electron. Lett.*, vol. 38, pp. 798–800, July 2002.

[94] H. Ito, F. Nakajima, T. Furuta, K. Yoshino, Y. Hirota, and T. Ishibashi, "Photonic terahertz-wave generation using an antenna-integrated uni-travelling-carrier photodiode," *Electron. Lett.*, vol. 39, pp. 1828–1829, Dec. 2003.

[95] S. Verghese, K. A. McIntosh, S. M. Duffy, and E. K. Duerr, "Continuous-wave terahertz generation using photomixers," in *Terahertz Sources and Systems*, R. E. Miles, P. Harrison, and D. Lippens, Eds. Berlin, Germany: Kluwer, 2001, p. 157.

[96] A. Malcoci, A. Stöhr, S. Schultz, and D. Jäger, "Optical THz generation," in *Tech. Dig. Int. Topical Meeting Microwave Photonics*, 2003, pp. 179–182.

[97] H. Ito and T. Nagatsuma, "Ultrafast uni-traveling-carrier photodiodes for measurements and sensing systems," *Proc. SPIE*, vol. 4999, pp. 156–166, 2003.

[98] T. Monitani, A. Hirata, and T. Nagatsuma, "A broadband 120-GHz Schottky-diode receiver for 10-Gb/s wireless links," *IEICE Trans. Electron.*, vol. E86-C, pp. 1501–1505, 2003.

[99] A. Hirata, T. Kosugi, T. Shibata, T. Furuta, H. Ito, and T. Nagatsuma, "Waveguide-output photodiode module integrated with HEMT amplifier for 10-Gb/s wireless link," in *Tech. Dig. Int. Symp. Contemporary Photonics Technology*, 2004, pp. 63–64.

[100] T. Nagatsuma, A. Hirata, M. Harada, H. Ishii, K. Machida, T. Minotani, H. Ito, T. Kosugi, and T. Shibata, "Millimeter-wave photonic integrated circuit technologies for high-speed wireless communications applications," in *IEEE Int. Solid-State Circuits Conf. Dig. Tech. Papers*, 2004, pp. 448–449.

[101] K. Ohata, K. Maruhashi, M. Ito, S. Kishimoto, K. Ikuina, T. Hashiguchi, N. Takahashi, and S. Inagawa, "Wireless 1.25 Gb/s transceiver module at 60 GHz-band," in *IEEE Int. Solid-State Circuits Conf. Dig. Tech. Papers*, 2002, pp. 298–299.

[102] Y. Doi, S. Fukushima, K. Takahata, K. Yoshino, and H. Ito, "Compact 60-GHz photonic millimeter-wave emitter module for fiber radio link," in *Tech. Dig. Int. Topical Meeting Microwave Photonics*, 2002, pp. 65–68.

[103] K. Takahata, Y. Muramoto, S. Fukushima, T. Furuta, and H. Ito, "Monolithically integrated millimeter-wave photonic emitter for 60-GHz fiber-radio applications," in *Tech. Dig. Int. Topical Meeting Microwave Photonics*, 2000, pp. 229–232.

[104] M. Tsuchiya and T. Hoshida, "Nonlinear photodetection scheme and its system application to fiber-optic millimeter-wave wireless down-links," *IEEE Trans. Microwave Theory Tech.*, vol. 47, pp. 1342–1350, July 1999.

[105] H. Fushimi, T. Furuta, T. Ishibashi, and H. Ito, "Photoresponse nonlinearity of a uni-traveling-carrier photodiode and its application to the optoelectronic mm-wave mixing in 60 GHz band," *Jpn. J. Appl. Phys.*, vol. 43, pp. L966–L968, July 2004.

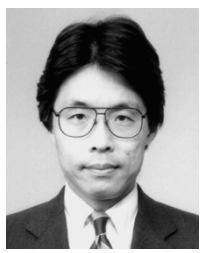

Hiroshi Ito (M'92–SM'03) received the B.S. and M.S. degrees in physics and the Ph.D. degree in electrical engineering from Hokkaido University, Japan, in 1980, 1982, and 1987, respectively.

Since joining NTT Electrical Communication Laboratories, Musashino, Tokyo, Japan, in 1982, he has been involved in research on growth and characterization of III-V compound semiconductors using MBE and MOCVD, and their applications to GaAs- and InP-based heterojunction devices such as bipolar transistors (HBTs), field effect transistors (HFETs), lasers, photodiodes, and integrated optical gates based on electro-absorption modulators. From 1991 to 1992, he was at Stanford University as a Visiting Scientist. He is currently a Group Leader at NTT Photonics Laboratories, Kanagawa, Japan. His research interests include ultrafast photonic devices for high-bit-rate and millimeter-/submillimeter-wave systems.

Dr. Ito is a member of the Institute of Electronics, Information and Communication Engineers (IEICE), the Japan Society of Applied Physics, and the Physical Society of Japan.

Satoshi Kodama was born in Ohtsu, Japan, in 1968. He received the B.E. degree in information engineering, and the M.E. and Ph.D. degrees in electrical engineering from Hokkaido University, Sapporo, Japan, in 1991, 1993, and 1996, respectively.

In 1996, he joined LSI laboratories, Nippon Telegraph and Telephone Co., Atsugi, Japan. He is currently a Senior Research Engineer at the Photonics Laboratories, Nippon Telegraph and Telephone Co., Kanagawa, Japan. His research interests include integrated advanced optelectronics devices.

Dr. Kodama is a member of the Institute of Electronics, Information and Communication Engineers (IEICE) of Japan, and the Japan Society of Applied Physics.

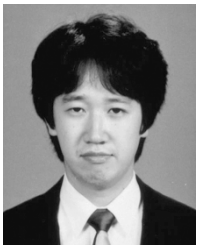

Yoshifumi Muramoto was born in Tokushima, Japan, on March 15, 1967. He received the B.E. and M.E. degrees from Osaka Prefecture University, Osaka, Japan, in 1990 and 1992, respectively.

In 1992, he joined NTT Opto-Electronics Laboratories. He has been engaged in research of monolithically integrated photoreceivers and high-speed photodetectors.

Mr. Muramoto is a member of the Institute of Electronics, Information and Communication Engineers (IEICE) of Japan, and the Japan Society of Applied Physics.

Tomofumi Furuta was born in Tokyo, Japan, in 1958. He received the B.S. and M.S. degrees from Tokyo University of Agriculture and Technology, in 1981 and 1983, respectively, and the Ph.D. degree from the University of Tokyo in 1986, all in the electrical engineering.

In 1986, he joined the NTT Laboratories, Kanagawa, Japan. He has been engaged in the research of semiconductor physics and devices.

Dr. Furuta is a member of the Japan Society of Applied Physics.

Tadao Nagatsuma (M'93–SM'02) received the B.S., M.S., and Ph.D. degrees in electronic engineering from Kyushu University, Fukuoka, Japan, in 1981, 1983, and 1986, respectively.

In 1986, he joined the Nippon Telegraph and Telephone Corporation (NTT), Atsugi Electrical Communications Laboratories, Kanagawa, Japan. From 1999 to 2002, he was a Distinguished Technical Member at NTT Telecommunications Energy Laboratories. He is currently a Group Leader at NTT Microsystem Integration Laboratories, Kanagawa. His research includes ultrahigh-speed electronics and millimeter-wave photonics and their application to sensors and communications.

Dr. Nagatsuma is a member of the Optical Society of America and the Institute of Electronics, Information and Communication Engineers (IEICE), Japan. He was the recipient of the 1989 Young Engineers Award presented by the IEICE, the 1992 IEEE Andrew R. Chi Best Paper Award, the 1997 Okochi Memorial Award, the 1998 Japan Microwave Prize, the 2000 Minister's Award of the Science and Technology Agency, and the 2002 Asia Pacific Microwave Conference APMC Prize.

Tadao Ishibashi (M'89–SM'03) was born in Sapporo, Japan, in 1949. He received Ph.D. degrees in applied physics from Hokkaido University, Japan, in 1986.

Since joining NTT Laboratories, Tokyo, Japan, in 1973, he has been involved in research of semiconductor devices and related material processing. His work included submillimeter-wave Si IMPATT diode oscillators, LPE growth of InP–InGaAs materials and their application to field effect transistors, MBE growth of MQW structures for laser diodes, GaAs- and InP-based heterostructure bipolar transistor ICs, ultrahigh-speed photodetectors, and integrated optical switches based on electroabsorption modulators. During 1991 to 1992, he was a Visiting Scientist at Max-Planck-Institute, Stuttgart, Germany. In 2001, he moved to NTT Electronics, Kanagawa, Japan, and is currently working on semiconductor optical components for fiber-optic systems.